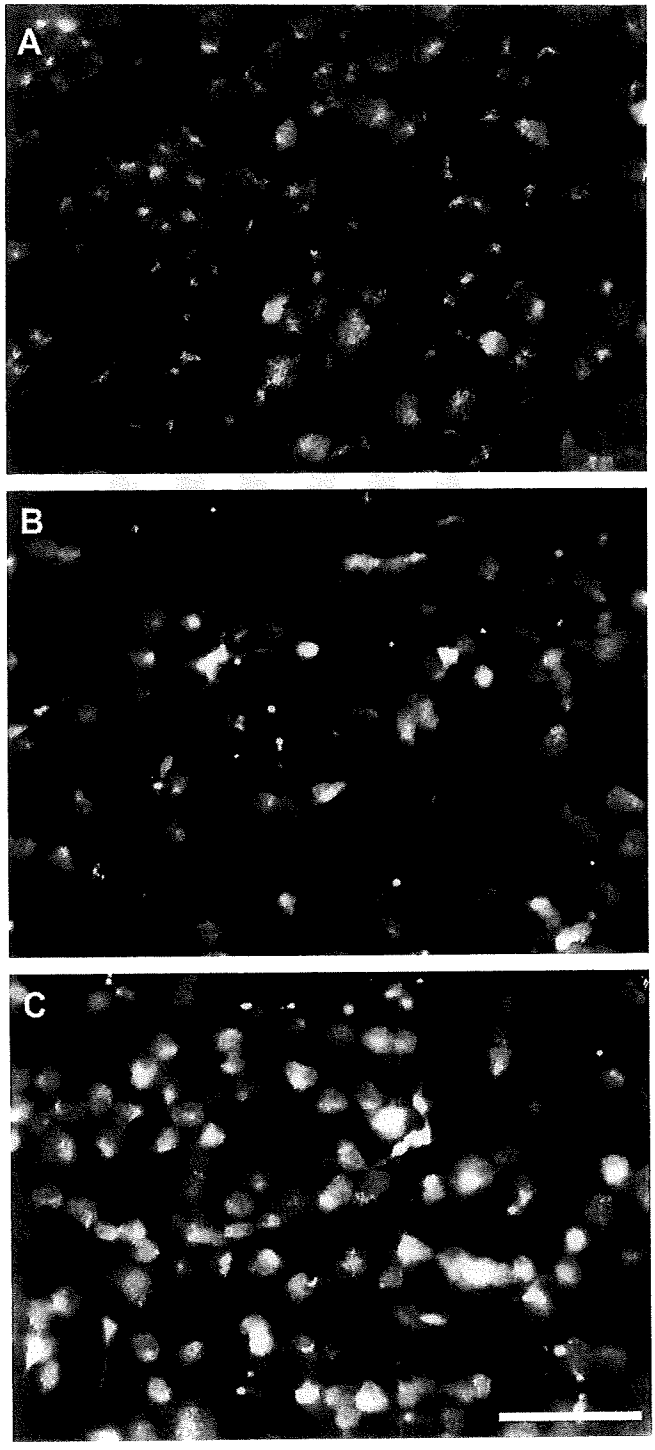

Fig. 1. Representative photographs of Fluorogold (FG)-labeled RGCs in flat-mounted retinas: intact (A), 7 days after ON transection without TES (B), ON transection with TES (C). All images were obtained from an approximately 1 mm temporal to the optic disk in each retina. A: In an intact retina, FG-labeled RGCs can be seen to have round-shaped soma with punctuate fluorescence of FG in their cytoplasm. B: In the retina 7 days after ON transection, the number of FG-labeled RGCs is markedly lower than that of RGCs in the intact retina, and debris of dead cells can be seen. C: In the retina 7 days after ON transection with TES (100 μA, 1 ms/phase, 20 Hz, 60 min), the number of surviving RGCs is strongly enhanced by TES, and many FG-labeled RGCs appeared to be similar to those in intact retinas. Scale bar = 100 μm.

Our overall results showed that TES promoted the survival of axotomized RGCs and the degree of neuroprotection depended on the pulse durations. Examination of the retinas following ON transection and TES showed many RGCs, whose shapes resembled those of the RGCs in intact retinas, had survived (Fig. 1C). The mean density of RGCs following TES of 0.5 ms/phase duration was significantly increased to 1639 ± 215 cells/mm^2 which was 69.5% of intact retinas ($P < 0.001$ vs sham stimulation; $n = 6$; Fig. 2A). TES of 1, 2 and 3 ms/phase pulse durations further increased the density up to 85.4%, 85.3% and 81.6%, respectively, of the intact retinas ($P < 0.001$; $n = 6$ each; Fig. 2A). Although TES of 5 ms/phase duration significantly increased the density of RGCs to 72.3% ($n = 6$) of that in sham stimulation, the neuroprotective effect was significantly lower than the maximum effect of 1 ms/phase ($P = 0.002$; $n = 6$; Fig. 2A).

3.2. Effect of current intensity on neuroprotection of axotomized RGCs

The mean RGC density in the retinas following TES at a current intensity of 50 μA was 1624 ± 55 cells/mm^2 ($n = 6$) which is 68.9% of intact retinas. This density was not significantly different from that in the sham stimulated retinas (Fig. 2B). However when the TES was increased to 100 μA and 200 μA, there was a significant increase in the density to 85.4% and 80.0%, respectively, of intact retinas ($P < 0.05$; $n = 6$ each). An increase of TES to 300 μA and 500 μA resulted in a decrease in the mean RGC densities to 70.0% and 64.5%, respectively, of intact retinas. These values were not significantly different from that of the sham stimulated eyes (Fig. 2B).

3.3. Effect of electric charge (intensity × duration) on neuroprotection of axotomized RGCs

The magnitude of the electric charge/phase, i.e., current intensity × pulse duration in coulombs has been identified as one of the factors that determine the effectiveness of ES in being neuroprotective in neural tissues. We compared the difference in the neuroprotective ability between increases of pulse duration to increases of current intensity. An increase in the current intensity decreased the number of RGCs more than an increase of pulse duration (Fig. 2C). There were significant differences in the number of RGCs between the survival effect with increases of current intensity and increases of pulse duration at more than 300 μC/phase ($^*P = 0.006$, $^{**}P = 0.002$; Fig. 2C).

3.4. Effect of frequency of stimulation on neuroprotection of axotomized RGCs

The mean RGC densities seven days after ON transection with sham stimulation and TES at 5 different frequencies are shown in Fig. 3. At 20 Hz, the mean RGC density was 85.0% of intact retinas which was significantly higher than that in the sham stimulated retinas ($P < 0.001$; $n = 6$). At 50 and 100 Hz, the mean RGC densities decreased to 73.1% and 68.5% respectively ($n = 6$ each), but these values were also significantly higher than that of sham stimulation. At 100 Hz the percentage of RGCs surviving after TES was significantly lower than that after 20 Hz TES ($P = 0.004$). Thus the optimal TES frequency was 20 Hz. The survival rates after TES of 5 Hz and 1 Hz were not significantly different from that at 20 Hz, 80.0% and 84.3%, respectively, of intact retinas ($n = 6$ each, $P < 0.001$ vs Sham stimulation). On the other hand, TES at 0.5 Hz did not have a significant protection, 60.8% (Fig. 3; $n = 6$).

3.5. Effect of waveform on neuroprotection of axotomized RGCs

The neuroprotective effects of the three types of waveforms with equal charge-balance were different (Fig. 4A). TES with Type II, symmetric waveforms led to a significantly increased survival of 85% compared to the sham stimulation, while asymmetrical

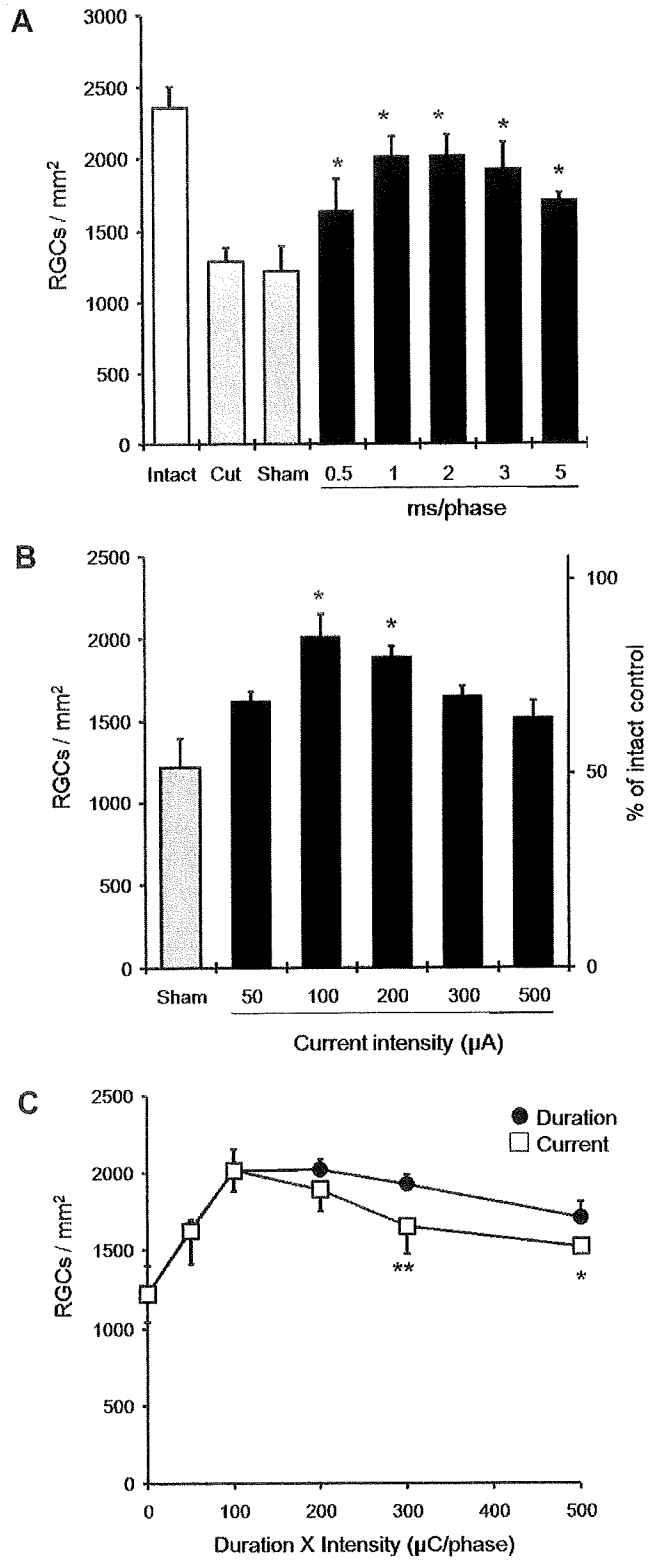

Fig. 2. Effects of pulse duration and current intensity of TES on the survival of axotomized RGCs 7 days after ON transection. A: Pulse duration-dependent neuroprotective effect of TES on RGC survival. TES (current intensity: 100 μA; frequency: 20 Hz) for 1 h was applied immediately after the ON was transected. The density of the FG-labeled RGCs/mm^2 is presented as the means ± SDs. Seven days after ON transection, the density of the RGCs is reduced to 54% of the control (Cut group). In the sham-treated animals (no electrical stimulation after ON transection), the density decreased to 53% of that of the intact control retina (Sham group). The RGC density in all five groups with TES (0.5, 1, 2, 3, and 5 ms/phase pulse duration) was significantly higher than in the sham group. Statistical analysis was made by one-way ANOVA followed by Tukey test ($P < 0.001$, $^*P < 0.001$ compared with sham). B: Current intensity-dependent neuroprotective effect of TES on RGC survival 7 days after ON transection. TES (pulse duration: 1 ms/phase; frequency: 20 Hz) for 1 h was applied immediately after ON transection. TES at 100 μA and 200 μA significantly increased the mean RGC densities compared with sham stimulation. Statistical analysis was made by Kruskal–Wallis One-Way Analysis of Variance on Ranks followed by Dunn's method ($P < 0.001$, $^*P < 0.05$ compared with sham). C. Comparison of neuroprotective effect of TES with pulse duration change and that with current intensity change 7 days after ON transection. The survival effect by current intensity significantly decreases as compared with that by pulse duration (more than 300 μC/phase) (*t* test, $^{**}P = 0.002$, $^*P = 0.006$).

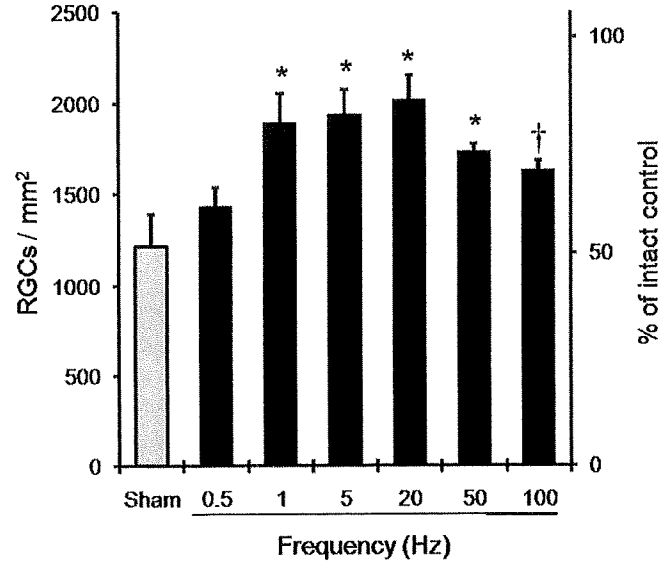

Fig. 3. Frequency-dependent neuroprotective effect of TES on axotomized RGCs 7 days after ON transection. TES (current intensity 100 μA; pulse duration 1 ms/phase) for 1 h was applied immediately after ON transection. TES at 1–20 Hz exerted the most significant effect on RGC survival; the mean densities of RGCs at 1–20 Hz exerted the most significant effect on RGC survival; the mean densities of RGCs at 1–20 Hz was significantly higher than the sham stimulation group ($P < 0.005$). Statistical analysis between the sham stimulation and ES groups was performed using one-way ANOVA followed by Tukey test ($P < 0.01$, $^*P < 0.005$, †$P < 0.001$ compared with sham).

waveforms of Type I led to a survival of 68.7% and Type III to 68.3% of intact retinas ($P < 0.001$; $n = 6$ each; Fig. 4B).

Next we examined the effect of the addition of inter-pulse interval to symmetrical pulses on the survival-promoting effect on RGCs (Fig. 4C). As the inter-pulse interval was increased, the survival rate of RGCs significantly decreased from 85% to 62% ($P < 0.001$; $n = 6$ each; Fig. 4D).

3.6. Stimulation duration on neuroprotection of axotomized RGCs

TES for 30 min significantly increased the survival of RGCs to 1802 ± 111 cells/mm^2 ($n = 6$) which is 76.8% of intact retinas ($P < 0.001$ vs sham stimulation). On the other hand, after TES for 10 min, the mean RGC density was 1398 ± 124 cells/mm^2 ($n = 6$, 59.3% of intact retinas), which was not significantly different than that of the sham stimulated retinas (Fig. 5).

3.7. Effect of repeated TES on neuroprotection of axotomized RGCs

The mean RGC density in retinas 14 days after ON transection with sham stimulation was 350 ± 216 cells/mm^2 ($n = 6$), which was 13.9% of intact retinas ($n = 6$; Fig. 6A,D). On the other hand, a single TES session (1× TES) significantly enhanced the survival of RGCs to 22.9% of intact retinas ($P < 0.001$ vs sham; $n = 6$; Fig. 6B,D). Four TES sessions (4× TES on days 0, 4, 7 and 10 after ON transection) further increased the number of RGCs to 47.1% of intact retinas ($P = 0.024$ vs 1× TES; $n = 6$; Fig. 6C,D).

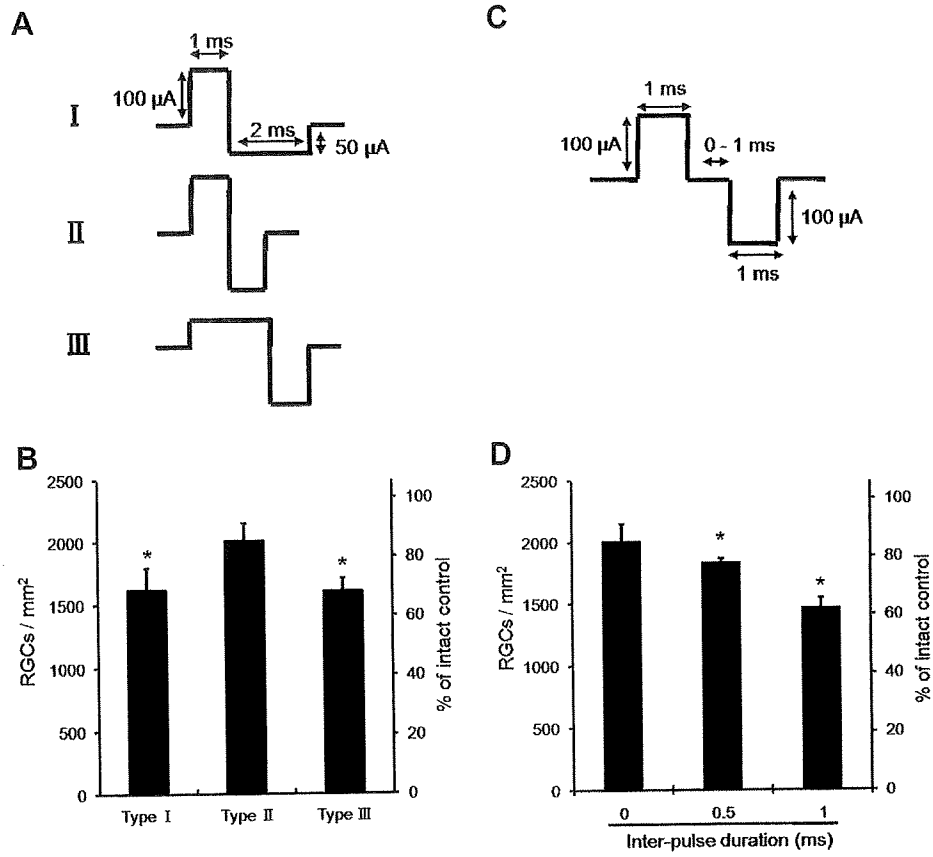

Fig. 4. Effects of waveforms of TES on the survival of axotomized RGCs 7 days after ON transection. A: Waveforms of the biphasic stimuli used in this study. Type I: Asymmetric rectangular pulse waveform (anodic first wave 100 μA, 1 ms/phase and cathodic second wave 50 μA, 2 ms/phase), Type II: Symmetric rectangular pulse waveform (100 μA, 1 ms/phase), Type III: Asymmetric rectangular pulse waveform (anodic first wave 50 μA, 2 ms/phase and cathodic second wave 100 μA, 1 ms/phase). All waves were charge-balanced. B: Neuroprotective effect of each waveform on axotomized RGCs 7 days after ON transection. TES with symmetric waveform (Type II) significantly increased the survival of RGCs more than asymmetric waveforms (Type I and Type III). Statistical analysis was performed using one-way ANOVA followed by Tukey test ($P < 0.001$, $^*P < 0.001$ compared with Type II). C: Waveform of a symmetric waveform with inter-pulse interval. D: Effect of inter-pulse interval on axotomized RGCs. The neuroprotective effect of TES on RGCs significantly decreased depending on the length of inter-pulse interval. Statistical analysis was performed using one-way ANOVA followed by Tukey test ($P < 0.001$, $^*P < 0.001$ compared with Type II without inter-pulse interval).

4. Discussion

Our results showed that the neuroprotective effect of TES on axotomized RGCs was dependent on the pulse duration, current intensity, frequency, stimulation duration, waveform, and the number of stimulation sessions.

4.1. Current charge (pulse duration × intensity)

The neuroprotective effect of TES was dependent on both the pulse duration and current intensity. There was a range of optimal pulse durations and current intensities, and an increase of the pulse duration or current intensity over the optimal range decreased the survival-promoting effect. On the other hand, the density of the electric charge, which is the production of current intensity and pulse duration, determined the extent of neural tissue damage (Yuen et al., 1981; McCreery et al., 1990; Harnack et al., 2004; Nakauchi et al., 2007). We found that there was a significant difference in neuroprotective effect of pulse duration and current intensity, on the basis of the same amount of electric charges (more than 300 μC/phase). In a retinal prosthesis study using supra-choroidal–transretinal stimulation (STS), the threshold of electric charge for the retinal safety was lower with shorter pulse durations even with the same amount of electric charge (Nakauchi et al., 2007). This is similar to our present results. Because the electric charge rate within an unit time became larger with an increase of

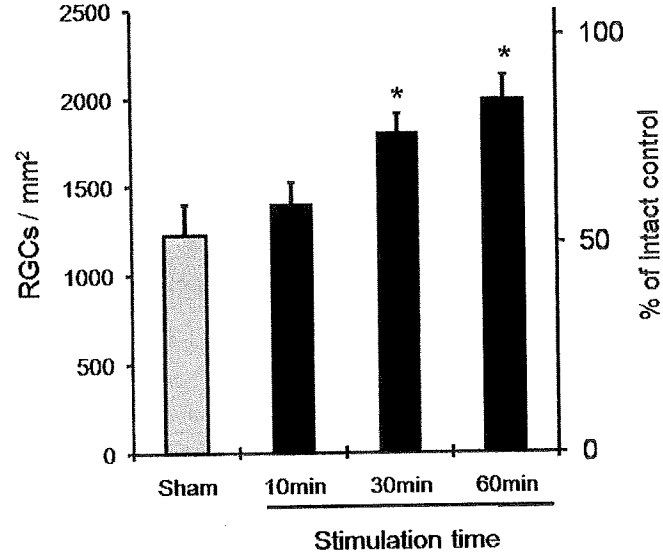

Fig. 5. Effect of stimulation duration on neuroprotection of axotomized RGCs. TES (current intensity: 100 μA; pulse duration: 1 ms/phase; frequency: 20 Hz) was applied immediately after ON transection. In the 10 min ES group, the mean density of RGCs was not significantly different from that in the sham group. In the 30 and 60 min groups, the mean density was significantly higher than that in the sham group ($P < 0.001$; each $n = 6$). Statistical analysis among the groups was performed using one-way ANOVA ($P < 0.001$) followed by Tukey test ($^*P < 0.001$ compared with the sham group).

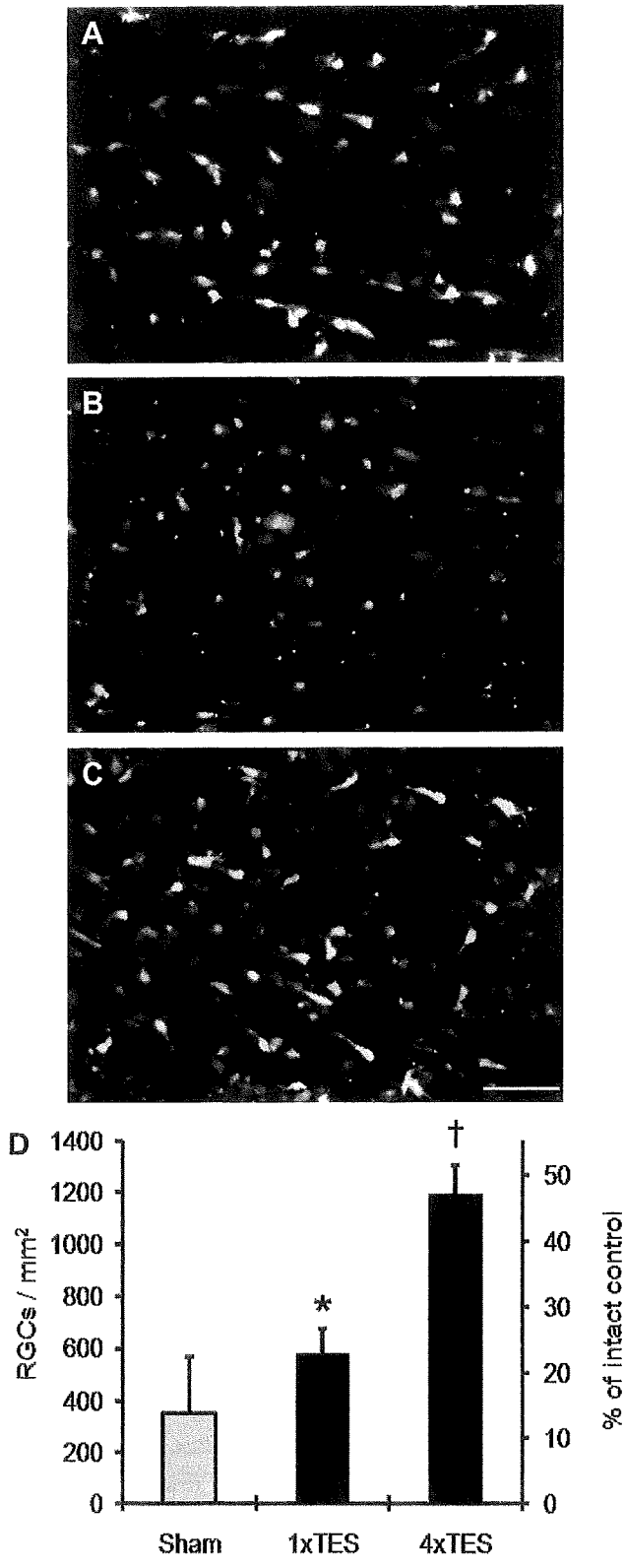

Fig. 6. Effect of repeated TES on the survival of RGCs 14 days after ON transection. Fluorescence photomicrographs of retinas 14 days after ON transection with sham TES (A), with single TES (B) and 4 times TES (C). Only a few FG-labeled RGCs are present 14 days after ON transection with sham stimulation (A). On the other hand single TES increased the viable RGCs (B), and 4× TES further increased the viable RGCs than 1× TES (C), Scale bar = 100 μm. Mean density of RGCs 14 days after ON transection with sham TES was much lower than that in the retina 7 days after ON transection. Although the mean density of RGCs 14 days after ON transection with 1× TES was also lower than that of RGCs 7 days after ON transection with TES, the density remained significantly higher than that with sham TES 14 days after ON transection ($P = 0.02$). Moreover 4× TES significantly increased the surviving RGCs more than single TES 14 days after ON transection ($P < 0.001$). One-way ANOVA: $P < 0.001$, followed by Tukey test: $^{*}P = 0.02$, $^{\dagger}P < 0.001$ comparing with sham group (D).

current intensity than with an increase of pulse duration, the increase of electric current may cause greater tissue damage even if the same amount of electric charge/phase is given. Therefore the neuroprotective effect may be lower with an increase of current intensity than that of pulse duration.

4.2. Frequency-dependent effect of TES on RGC survival

TES of 1–20 Hz frequency had the greatest neuroprotection on RGCs. On the other hand, when the ON stump is stimulated thus stimulating the axons of the RGCs, 20 Hz of ES was the most optimal frequency (Okazaki et al., 2008). It is possible that TES stimulates not only RGCs but also other retinal cells such as the Müller cells to exert its neuroprotective effects. In fact, our earlier study showed that 20 Hz TES increased the expression of IGF-1 in Müller cells *in vivo* (Morimoto et al., 2005) and direct 20 Hz ES to the cultured Müller cells also increased the expression of insulin-like growth factor-1 (IGF-1), brain derived neurotrophic factor (BDNF) and fibroblast growth factor 2 (FGF2) in these cells (Sato et al., 2008a,b,c). Therefore TES might have the wider range of optimal frequencies than the direct stimulation of the ON stump.

In other neural tissues, different frequencies were reported to be optimal. For example, after crushing the spinal cord *in vivo*, ES at 20 Hz also promoted axonal regeneration of the motoneurons (Al-Majed et al., 2000a,b). On the other hand, for cochlear implants high frequency (300 pps) of ES promoted a greater survival of ototoxic spiral ganglion cells (SGCs) than low frequency (30 pps) of ES *in vivo* (Leake et al., 2008). *In vitro* study, not low frequency (20 Hz) but high frequency (50 or 100 Hz) of ES promoted the secretion of BDNF from hippocampal neurons or primary sensory neurons (Balkowiec and Katz, 2000, 2002). ES of dorsal root ganglion (DRG) axons at 20 Hz promoted greater axonal regeneration than 200 Hz (Udina et al., 2008). Thus the optimal frequency of ES to have neuroprotective effects differs for different types of neurons and nervous systems. Because neurons and glial cells have various voltage-sensitive ion channels for each cells, the activation of ion channels may depend on the frequency of ES. For example, Müller cells have voltage-sensitive L-type Ca channel (Xu et al., 2002). We have demonstrated that 20 Hz ES activates voltage-sensitive L-type Ca channels to increase the expression of the mRNAs of IGF-1 and BDNF in cultured Müller cells (Sato et al., 2008a,b). In hippocampal neurons, 100 Hz ES activates the N-type Ca channels to make hippocampal neurons release BDNF (Brosenitsch and Katz, 2001). Another possibility is that high frequency of ES induces greater tissue damage. In the cat's sciatic nerve, ES at 100 Hz and 50 Hz cause the severe neural damage, although ES at 20 Hz induces little or no neural damage (McCreery et al., 1995). Thus it is important to select the suitable frequency of ES applied for each type of neuron.

4.3. Effect of waveforms on the TES-induced neuroprotective effect

TES with symmetric pulse waves increased the number of surviving RGCs more than TES with asymmetric pulse waves, although both pulse waves were charge-balanced. Moreover, longer inter-pulse intervals resulted in less surviving RGCs than TES with no inter-pulse intervals. It is possible that the electric charge might not be balanced well by asymmetrical pulses to cause the tissue damage. Or it is possible that the increase in the inter-pulse interval than the safety limit, might cause the tissue damage. In cochlear

implants, the threshold of auditory nerve response evoked by ES with asymmetric pulse waves is lower than that by ES with symmetric pulse waves and the threshold of auditory nerve response evoked by long inter-pulse intervals is lower than that by the ES without inter-pulse intervals (Macherey et al., 2006). The effects of asymmetrical or symmetrical pulses with long inter-pulse intervals were similar to monophasic pulses (Macherey et al., 2006). These pulses might lead to neural damage with the lower electric charge than the symmetric pulses.

4.4. Stimulation time-dependent effect of TES on RGC survival

TES for 10 min immediately after ON transection did not increase the number of surviving RGCs, but that for 30 min did. This result is similar to that following ES of the transected ON stump (Okazaki et al., 2008). These results indicate that ES to RGCs may influence the intrinsic survival signal or the death signal. It may take more than 30 min of intervention to obtain some survival signals. Further investigation is needed to determine what kind of signals are being induced.

4.5. Single TES vs repeated TES for long-lasting neuroprotection

Fourteen days after ON transection, the densities of surviving RGCs in the retinas with single TES (1× TES) were still higher than in the control retinas without TES. And repetitive TES (4× TES) increased the number of surviving RGCs more than 1× TES. These results indicate that repeated TES has cumulative neurotrophic effects on the long term survival of RGCs. In fact we have demonstrated that TES up-regulates the expression of the mRNA and protein of IGF-1 to rescue axotomized RGCs (Morimoto et al., 2005). Our results suggest that IGF-1 induced by TES might be cumulative and have neuroprotective effects of RGCs continuously for 2 weeks. The mechanism of repetitive TES on the longer term survival of RGCs should be investigated in the future.

5. Conclusions

We performed a systematic analysis of the neuroprotective effect of different stimulus parameters of TES on axotomized RGCs. We concluded that the optimal parameter of TES on the neuroprotection of RGCs are: current intensity of 100–200 μA, pulse duration of 1–3 ms/phase, frequency of 1–20 Hz, stimulation duration of 30–60 min, symmetrical pulse waves without inter-pulse intervals, and repeated stimulations. It is important that stimulation with these optimal parameters with low electric power, is applied for the overall period to maintain long term survival of RGCs. These findings should serve as guideline for ES in humans.

Acknowledgments

We thank Professor Yasuo Tano for helpful advice and various supports.

This work was supported by a Health Sciences Research Grant (H19-sensory-001) from the Ministry of Health, Labour and Welfare, Japan.

References

Al-Majed, A.A., Neumann, C.M., Brushart, T.M., Gordon, T., 2000a. Brief electrical stimulation promotes the speed and accuracy of motor axonal regeneration. J. Neurosci. 20, 2602–2608.

Al-Majed, A.A., Brushart, T.M., Gordon, T., 2000b. Electrical stimulation accelerates and increases expression of BDNF and trkB mRNA in regenerating rat femoral motoneurons. Eur. J. Neurosci. 12, 4381–4390.

Balkowiec, A., Katz, D.M., 2000. Activity-dependent release of endogenous brain-derived neurotrophic factor from primary sensory neurons detected by ELISA in situ. J. Neurosci. 20, 7417–7423.

Balkowiec, A., Katz, D.M., 2002. Cellular mechanisms regulating activity-dependent release of native brain-derived neurotrophic factor from hippocampal neurons. J. Neurosci. 22, 10399–10407.

Brosenitsch, T.A., Katz, D.M., 2001. Physiological patterns of electrical stimulation can induce neuronal gene expression by activating N-type calcium channels. J. Neurosci. 21, 2571–2579.

Fields, R.D., Neale, E.A., Nelson, P.G., 1990. Effects of patterned electrical activity on neurite outgrowth from mouse sensory neurons. J. Neurosci. 10, 2950–2964.

Fujikado, T., Morimoto, T., Matsushita, K., Shimojo, H., Okawa, Y., Tano, Y., 2006. Effect of transcorneal electrical stimulation in patients with nonarteritic ischemic optic neuropathy or traumatic optic neuropathy. Jpn. J. Ophthalmol. 50, 266–273.

Goldberg, J.L., Espinosa, J.S., Xu, Y., Davidson, N., Kovacs, G.T., Barres, B.A., 2002. Retinal ganglion cells do not extend axons by default: promotion by neurotrophic signaling and electrical activity. Neuron 33, 689–702.

Grumbacher-Reinert, S., Nicholls, J., 1992. Influence of substrate on retraction of neurites following electrical activity of leech Retzius cells in culture. J. Exp. Biol. 167, 1–14.

Harnack, D., Winter, C., Meissner, W., Reum, T., Kupsch, A., Morgenstern, R., 2004. The effects of electrode material, charge density and stimulation duration on the safety of high-frequency stimulation of the subthalamic nucleus in rats. J. Neurosci. Methods 138, 207–216.

Inomata, K., Shinoda, K., Ohde, H., Tsunoda, K., Hanazono, G., Kimura, I., Yuzawa, M., Tsubota, K., Miyake, Y., 2007. Transcorneal electrical stimulation of retina to treat longstanding retinal artery occlusion. Graefes. Arch. Clin. Exp. Ophthalmol. 245, 1773–1780.

Leake, P.A., Stakhovskaya, O., Hradek, G.T., Hetherington, A.M., 2008. Factors influencing neurotrophic effects of electrical stimulation in the deafened developing auditory system. Hear. Res. 242, 86–99.

Linden, R., 1994. The survival of developing neurons: a review of afferent control. Neuroscience 58, 671–682.

Macherey, O., van, Wieringen, A., Carlyon, R.P., Deeks, J.M., Wouters, J., 2006. Asymmetric pulses in cochlear implants: effects of pulse shape, polarity, and rate. J. Assoc. Res. Otolaryngol. 7, 253–266.

McCreery, D.B., Agnew, W.F., Yuen, T.G., Bullara, L., 1990. Charge density and charge per phase as cofactors in neural injury induced by electrical stimulation. IEEE Trans. Biomed. Eng. 37, 996–1001.

McCreery, D.B., Agnew, W.F., Yuen, T.G., Bullara, L., 1995. Relationship between stimulus amplitude, stimulus frequency and neural damage during electrical stimulation of sciatic nerve of cat. Med. Biol. Eng. Comput. 33, 426–429.

Mennerick, S., Zorumski, C.F., 2000. Neural activity and survival in the developing nervous system. Mol. Neurobiol. 22, 41–54.

Meyer-Franke, A., Wilkinson, G.A., Kruttgen, A., Hu, M., Munro, E., Hanson Jr., M.G., Reichardt, L.F., Barres, B.A., 1998. Depolarization and cAMP elevation rapidly recruit TrkB to the plasma membrane of CNS neurons. Neuron 21, 681–693.

Miyake, K., Yoshida, M., Inoue, Y., Hata, Y., 2007. Neuroprotective effect of transcorneal electrical stimulation on the acute phase of optic nerve injury. Invest. Ophthalmol. Vis. Sci. 48, 2356–2361.

Morimoto, T., Miyoshi, T., Fujikado, T., Tano, Y., Fukuda, Y., 2002. Electrical stimulation enhances the survival of axotomized retinal ganglion cells in vivo. Neuroreport 13, 227–230.

Morimoto, T., Miyoshi, T., Matsuda, S., Tano, Y., Fujikado, T., Fukuda, Y., 2005. Transcorneal electrical stimulation rescues axotomized retinal ganglion cells by activating endogenous retinal IGF-1 system. Invest. Ophthalmol. Vis. Sci. 46, 2147–2155.

Morimoto, T., Fujikado, T., Choi, J.S., Kanda, H., Miyoshi, T., Fukuda, Y., Tano, Y., 2007. Transcorneal electrical stimulation promotes the survival of photoreceptors and preserves retinal function in royal college of surgeons rats. Invest. Ophthalmol. Vis. Sci. 48, 4725–4732.

Nakauchi, K., Fujikado, T., Kanda, H., Kusaka, S., Ozawa, M., Sakaguchi, H., Ikuno, Y., Kamei, M., Tano, Y., 2007. Threshold suprachoroidal–transretinal stimulation current resulting in retinal damage in rabbits. J. Neural Eng. 4, S50–S57.

Okazaki, Y., Morimoto, T., Sawai, H., 2008. Parameters of optic nerve electrical stimulation affecting neuroprotection of axotomized retinal ganglion cells in adult rats. Neurosci. Res. 61, 129–135.

Sato, T., Fujikado, T., Lee, T.S., Tano, Y., 2008a. Direct effect of electrical stimulation on induction of brain-derived neurotrophic factor from cultured retinal Müller cells. Invest. Ophthalmol. Vis. Sci. 49, 4641–4646.

Sato, T., Fujikado, T., Morimoto, T., Matsushita, K., Harada, T., Tano, Y., 2008b. Effect of electrical stimulation on IGF-1 transcription by L-type calcium channels in cultured retinal Müller cells. Jpn. J. Ophthalmol. 52, 217–223.

Sato, T., Lee, T.S., Takamatsu, F., Fujikado, T., 2008c. Induction of fibroblast growth factor-2 by electrical stimulation in cultured retinal Mueller cells. Neuroreport 19, 1617–1621.

Shen, S., Wiemelt, A.P., McMorris, F.A., Barres, B.A., 1999. Retinal ganglion cells lose trophic responsiveness after axotomy. Neuron 23, 285–295.

Udina, E., Furey, M., Busch, S., Silver, J., Gordon, T., Fouad, K., 2008. Electrical stimulation of intact peripheral sensory axons in rats promotes outgrowth of their central projections. Exp. Neurol. 210, 238–247.

Xu, H.P., Zhao, J.W., Yang, X.L., 2002. Expression of voltage-dependent calcium channel subunits in the rat retina. Neurosci. Lett. 329, 297–300.

Yuen, T.G., Agnew, W.F., Bullara, L.A., Jacques, S., McCreery, D.B., 1981. Histological evaluation of neural damage from electrical stimulation: considerations for the selection of parameters for clinical application. Neurosurgery 9, 292–299.

J Artif Organs (2009) 12:206–209
DOI 10.1007/s10047-009-0467-2

ORIGINAL ARTICLE

Hirokazu Sakaguchi, MD · Motohiro Kamei, MD
Takashi Fujikado, MD · Eiji Yonezawa,
Motoki Ozawa, MS · Carmen Cecilia-Gonzalez, MD
Orlando Ustariz-Gonzalez, MD
Hugo Quiroz-Mercado, MD · Yasuo Tano, MD

Artificial vision by direct optic nerve electrode (AV-DONE) implantation in a blind patient with retinitis pigmentosa

Abstract The purpose of this study was to evaluate the efficacy and safety of artificial vision by using a direct optic nerve electrode (AV-DONE) in a blind patient with retinitis pigmentosa (RP). This device, comprising three wire electrodes (0.05 mm in diameter), was implanted into the optic disc of a patient with RP with no light perception vision and the device was left implanted. Six months later, visual sensations were elicited by electrical stimulation through each electrode and the thresholds for the phosphene perception elicited by pulses of 0.25-ms duration/phase and a pulse frequency of 320 Hz were 30, 5, and 70 μA for each electrode. The phosphenes, which ranged in size from that of a match head to an apple, were round, oval, or linear, primarily yellow, and focally distributed. The area of the phosphenes changed when the electrical stimulation was supplied from different electrodes. No complications arose during the follow-up period. Localized visual sensations were produced in a blind patient with advanced RP, suggesting that our system could lead to the development of a useful visual prosthesis system.

Key words Human · Optic nerve · Retinitis pigmentosa · Visual sensation · Visual prosthesis

Received: January 10, 2009 / Accepted: May 13, 2009

H. Sakaguchi (✉) · M. Kamei · Y. Tano
Department of Ophthalmology, Osaka University Medical School, 2-2 Yamadaoka, E-7, Suita, Osaka 565-0871, Japan
Tel. +81-6-6879-3456; Fax +81-6-6879-3458
e-mail: sakaguh@ophthal.med.osaka-u.ac.jp

T. Fujikado
Department of Applied Visual Science, Osaka University Medical School, Suita, Japan

E. Yonezawa · M. Ozawa
NIDEK Co., Ltd., Gamagori, Japan

C. Cecilia-Gonzalez · O. Ustariz-Gonzalez · H. Quiroz-Mercado[1]
Vitreo and Retina Service, Asociacion Para Evitar la Ceguera, Mexico City, Mexico

Present address:
[1] University of Colorado and Denver Health Medical Center, Denver, CO, USA

Introduction

No treatment can restore vision to patients with retinitis pigmentosa (RP) once they have lost sight. In 1968, one group evaluated a visual prosthesis in a blind patient.[1] Dobelle et al.[2] reported in 1974 that a blind patient identified light using electrical stimulation from an electrode on the visual cortex, which leads to the realization that blind patients may recover vision. However, the cortical electrode and the intracranial surgery to implant it carry a risk of major complications. Many groups worldwide have suggested different approaches for restoring vision, with the retina or the optic nerve as new targets for stimulation.[3–15] Reportedly, 78% of the bipolar cells and 30% of the ganglion cells remain intact in the retinas of patients with advanced RP.[16] Therefore, it seems reasonable to target the remaining neural cells using electrical stimulation.

A group of researchers in Belgium implanted a spiral cuff electrode that supported four electrodes around the optic nerve of a blind patient with RP.[11,12] Whenever the pulse width, current intensity, the number, or the frequency of the stimulus train was changed, the patient perceived the corresponding phosphenes at different locations. Using these data, a map was constructed of the phosphenes that were stimulated, and an image was reproduced by selection of the corresponding phosphenes from the map. A volunteer with RP and no residual vision recognized letters with this system.[12]

Our group is also attempting to create visual prosthesis using a direct optic nerve electrode method.[17–19] We have tested electrical stimulation of the optic nerve with wire-type electrodes inserted transvitreously as an alternative to conventional visual prostheses. The efficacy and safety of this procedure have been reported in acute and long-term animal studies.[17–19] The purpose of the current study was to evaluate the usefulness and safety of our system during a preliminary clinical trial in a blind patient with RP.

Methods

Patient

The patient was a 35-year-old woman with RP with no light perception in the right eye and with light perception in the left eye. She had lost light perception from her right eye at least 4 years earlier. She had exotropia in her right eye. There were no other ocular diseases or systemic disorders that may have caused the visual loss. Approval from the Institutional Ethics Committee Board and informed consent from the patient were obtained for this research at Asociacion Para Evitar la Ceguera, Mexico City. This trial adhered to the tenets of the Declaration of Helsinki.

Electrode implantation

The surgery to implant the electrode was performed with the patient under general anesthesia. Phacoemulsification was performed and a silicone tube (Silascon, Kaneka Medix Corp. Tokyo, Japan) containing Parylene-coated platinum wires (each 0.05 mm in diameter) was sutured at the four scleral quadrants around the eyeball with a 5-0 suture. A small segment (0.5 mm) of the active tips of the wires were uncoated. After a standard three-port pars plana vitrectomy was performed, posterior vitreous detachment was confirmed. The wire bundle then was inserted into the scleral incision, which was 3.5 mm from the limbus. Three wire tips were inserted into the optic nerve using two vitreoretinal forceps. The tips were inserted within the optic disc area at a depth of 1.0–2.0 mm as far from the center as possible to avoid the vessels. The wires were inserted at the 12, 3, and, 9 o'clock positions. Another wire was left in the vitreous cavity as a reference electrode. After implantation, the wires around the eyeball were covered with Tenon and conjunctival tissue.

Before electrical stimulation, a peritomy was performed and the wires were uncovered. The end of each wire was connected to the stimulator. After the session, the wires were covered again with Tenon as well as conjunctival tissue and left in place for 6 months until the next session. The peritomy allowed access to the wires and connection to the stimulator for the second electrical stimulation session.

Electrical stimulation

Biphasic, cathodic-phase-first, electrical pulse trains of 1 s total duration were applied to the electrodes on two occasions: 1 day and 6 months postoperatively. The resulting phosphene perceptions were explored for threshold and localization in the visual field.

The duration of the stimulus pulses was 0.25 ms/phase and the frequency was 40 Hz, 160 Hz, or 320 Hz. The current was increased from 5 to 200 or 300 μA and then reduced from 200 or 300 down to 5 μA. No stimulation (0 μA) was applied at least once every ten stimulations to determine if the patient could differentiate electrically generated phosphenes from spontaneous phosphenes.

A beeping sound was issued in synchrony with each real or fake stimulation train. The patient was questioned about her phosphene perceptions, the clock position (1 to 12 o'clock), the distance from the center (central, mid, far), the color, and the size compared to a match head (a diameter of 3 mm), a pea (7 mm), a coin (20 mm), a ping-pong ball (40 mm), a baseball (70 mm), and an apple (100 mm), all viewed at arm's length. Everyday conversational words were used to ensure correct communication with the patient, such that the positions of the phosphenes were described in polar coordinates of the visual field.[20] The threshold of the phosphene perception was identified as the stimulation current when more than 50% of the tests were positive for perception.

Results

Electrode implantation and follow-up

No complications occurred intraoperatively or during the follow-up period. The wires remained functionally stable for at least 6 months (Fig. 1).

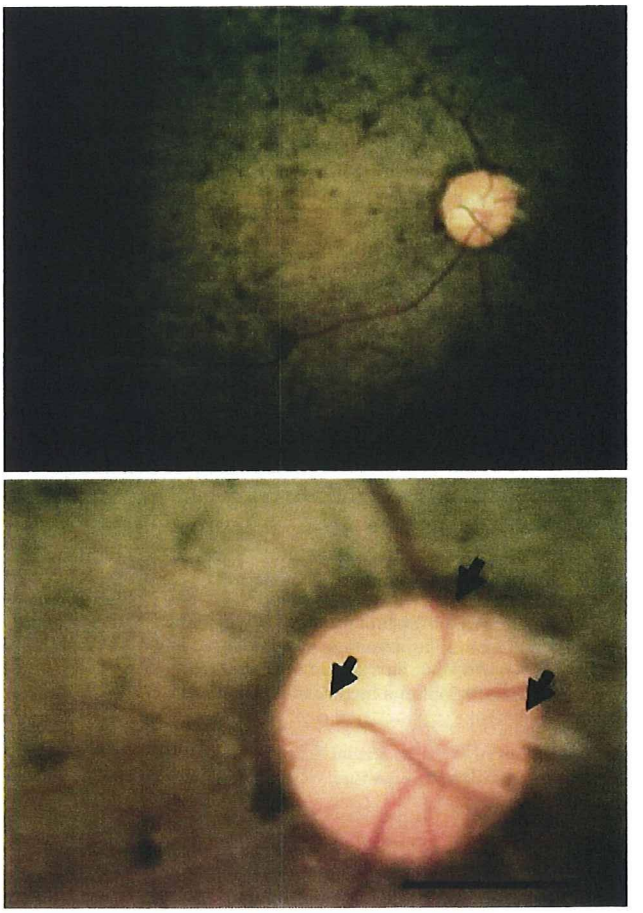

Fig. 1. The insertion of the platinum wire electrodes into the optic disc. *Upper*, three wire electrodes were inserted into the optic disc of the right eye, which had no light perception. *Lower*, the magnified image shows the electrode insertion sites (*arrows*). *Scale bar* 1.0 mm

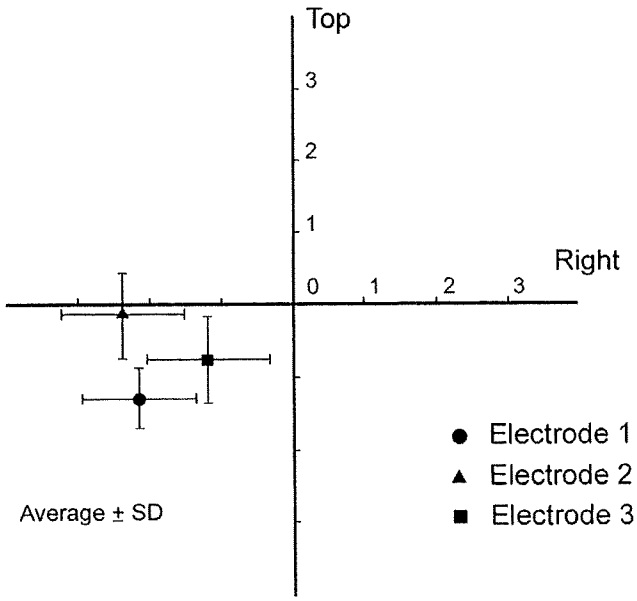

Fig. 2. The phosphenes generated by stimulation through each electrode were focally distributed in the visual field. The average central positions of the phosphenes clearly differ for each electrode

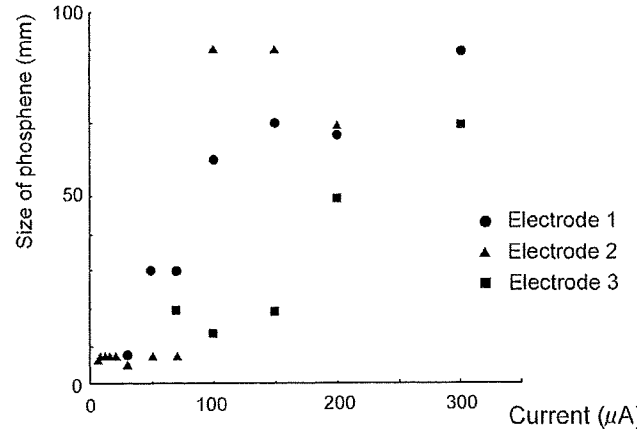

Fig. 3. The relationship between the size of the perceived phosphenes and the electrical stimulation. The sizes of the perceived phosphenes were significantly larger with higher electrical currents (Spearman rank order correlation: electrode 1 $r = 0.865$, $P < 0.05$; electrode 2 $r = 0.706$, $P < 0.05$; electrode 3 $r = 0.893$, $P < 0.05$)

Stimulation session

The patient identified electrically induced phosphenes from the first day after implantation. However, the data were unreliable because the patient could not distinguish clearly between artificial and spontaneous phosphenes, and she also seemed not to have understood the directions given to her. The entire stimulation session took about 3 h with the patient under topical anesthesia. Six months later, the identification of electrically induced phosphenes was reliable. The entire stimulation session took about 3 h using topical anesthesia.

The phosphenes generated by stimulation through each electrode were distributed focally in the visual field. The average phosphene center position differed for each electrode (Fig. 2). The size of the phosphenes was compared to objects ranging from a pea to an apple, from a match head to an apple, and from a pea to a baseball for electrodes 1, 2, and 3, respectively, all viewed at arm's length. The sizes of the perceived phosphenes were significantly larger with higher electrical currents (Spearman rank order correlation: electrode 1 $r = 0.865$, $P < 0.05$; electrode 2 $r = 0.706$, $P < 0.05$; electrode 3 $r = 0.893$, $P < 0.05$; Fig. 3). The patient described most of the 16 phosphenes from electrode 1 as yellow (14 yellow and 2 white) and all 20 and 10 phosphenes from electrodes 2 and 3, respectively, as yellow. The shapes of the phosphenes differed for each electrode. In total, 9 of the 16 phosphenes generated through electrode 1 were round and the other 7 were oval. Electrode 2 yielded 17 linear vertical phosphenes, 2 round phosphenes, and 1 linear horizontal phosphene. In total, 6 of the 10 phosphenes obtained with electrode 3 were linear horizontal in shape while 2 were linear vertical and the other 2 were round. No complications developed during the electrical stimulation session.

Discussion

We showed the feasibility of a new method to elicit artificial phosphene perceptions by electrical stimulation of optic nerve fibers with electrodes implanted through the optic disc in a blind patient with RP. A Belgian group also reported that a blind patient perceived phosphenes during electrical stimulation of the optic nerve fibers behind the eyeball.[11,12] These results clearly showed that the optic nerve fibers represent possible interface targets for visual prostheses.

The current study indicated that perceptions of a small phosphene, compared with a match head (about 23 arc min) or a pea (about 54 arc min) at arm's length, could be elicited by electrical stimulation of the optic nerve fibers. The sizes of the phosphenes significantly increased when stronger electrical currents were applied. This may result from recruitment of additional fibers around the electrode. The fact that small phosphenes were elicited suggests that a larger number of them could be induced independently using more electrodes in the optic disc, which would be an essential characteristic of our system. However, we should investigate further the effects of different electrical stimulation parameters. The shapes of the phosphenes differed for each electrode, which might indicate a combined effect of the local direction of the optic nerve fibers and the direction of insertion of the electrode wire.

The visual sensations were restricted to yellow in our trial. Humayun et al.[3] reported that four of five patients with light perception or no light perception with RP, retinal detachment, or age-related macular degeneration who could recognize localized phosphenes on electrical stimulation with an epiretinal electrode saw yellow or yellow–green

phosphenes, and one patient identified a white phosphene. Veraart et al.[11] showed that phosphenes produced by electrical stimulation with a cuff electrode around the optic nerve in a blind patient with RP were generally gold–yellow on the first day after surgery, and thereafter, blue, white, or plain yellow phosphenes were described, although the rates were not shown. The reason why the phosphenes were yellow in our trial is not well understood. This may result from electrical stimulation of the optic nerve or yellow may be the color associated with photoreceptor damage.

The current trial showed the possibility that our system may form the basis of a useful visual prosthesis. However, this system needs an active nerve fiber. Thus, diseases such as late-stage glaucoma and optic neuropathy, in which the nerve fibers are severely damaged, are not indicated for treatment with this system.

In the current study, the perceived position of the phosphenes in the visual field was determined by the electrode position in the optic nerve. With electrode contacts around the optic nerve periphery, a Belgian group reported that the position of the phosphenes in the visual field could be controlled by changing the stimulation train parameters including the pulse duration, current, frequency, and number.[11,12]

The current trial was limited by the absence of a transcutaneous transmission system. It was therefore impossible to draw a complete and accurate phosphene position map, which requires abundant data and consideration of the variability of subjective perceptions and a large number of parameters. A more advanced system is now under development that will allow us to complete this study in the near future.

To answer further questions about safety and efficacy, we need to observe more patients with this system, to perform more stimulation experiments to obtain more data, and to use a suitable system for energy and data supply to the electrodes.

Conclusion

Localized phosphene perceptions were elicited by stimulation of the optic disc electrode in a patient with advanced RP. Our data suggested that this system could lead to the development of a useful visual prosthesis system.

Acknowledgments This study was supported by a Grant-in-Aid for Scientific Research (A) from the Japan Society for the Promotion of Science, Japan, and a Health Sciences Research Grant from the Ministry of Health, Labor and Welfare, Japan. The authors thank J. Delbeke for helpful suggestions and critical reading of the manuscript.

References

1. Brindley GS, Lewin WS. The sensations produced by electrical stimulation of the visual cortex. J Physiol 1968;196:479–493
2. Dobelle WH, Mladejovsky MG, Girvin JP. Artificial vision for the blind: electrical stimulation of visual cortex offers hope for a functional prosthesis. Science 1974;183:440–444
3. Humayun MS, de Juan E Jr, Weiland JD, Dagnelie G, Katona S, Greenberg R, Suzuki S. Pattern electrical stimulation of the human retina. Vision Res 1999;39:2569–2576
4. Humayun MS, Weiland JD, Fujii GY, Greenberg R, Williamson R, Little J, Mech B, Cimmarusti V, Van Boemel G, Dagnelie G, de Juan E. Visual perception in a blind subject with a chronic microelectronic retinal prosthesis. Vision Res 2003;43:2573–2581
5. Chow AY, Chow VY. Subretinal electrical stimulation of the rabbit retina. Neurosci Lett 1997;225:13–16
6. Zrenner E, Miliczek KD, Gabel VP, Graf HG, Guenther E, Haemmerle H, Hoefflinger B, Kohler K, Nisch W, Schubert M, Stett A, Weiss S. The development of subretinal microphotodiodes for replacement of degenerated photoreceptors. Ophthalmic Res 1997;29:269–280
7. Zrenner E, Stett A, Weiss S, Aramant RB, Guenther E, Kohler K, Miliczek KD, Seiler MJ, Haemmerle H. Can subretinal microphotodiodes successfully replace degenerated photoreceptors? Vision Res 1999;39:2555–2567
8. Zrenner E. Will retinal implants restore vision? Science 2002;295: 1022–1025
9. Rizzo JF III, Wyatt J, Humayun M, de Juan E, Liu W, Chow A, Eckmiller R, Zrenner E, Yagi T, Abrams G. Retinal prosthesis: an encouraging first decade with major challenges ahead. Ophthalmology 2001;26:13–14
10. Rizzo JF III, Wyatt J, Loewenstein J, Kelly S, Shire D. Methods and perceptual thresholds for short-term electrical stimulation of human retina with microelectrode arrays. Invest Ophthalmol Vis Sci 2003;44:5355–5361
11. Veraart C, Raftopoulos C, Mortimer JT, Delbeke J, Pins D, Michaux G, Vanlierde A, Parrini S, Wanet-Defalque MC. Visual sensations produced by optic nerve stimulation using an implanted self-sizing spiral cuff electrode. Brain Res 1998;813:181–186
12. Veraart C, Wanet-Defalque MC, Gerard B, Vanlierde A, Delbeke J. Pattern recognition with the optic nerve visual prosthesis. Artif Organs 2003;27:996–1004
13. Sakaguchi H, Fujikado T, Fang X, Kanda H, Osanai M, Nakauchi K, Ikuno Y, Kamei M, Yagi T, Nishimura S, Ohji M, Yagi T, Tano Y. Transretinal electrical stimulation with a suprachoroidal multichannel electrode in rabbit eyes. Jpn J Ophthalmol 2004;48: 256–261
14. Nakauchi K, Fujikado T, Kanda H, Morimoto T, Choi JS, Ikuno Y, Sakaguchi H, Kamei M, Ohji M, Yagi T, Nishimura S, Sawai H, Fukuda Y, Tano Y. Transretinal electrical stimulation by an intrascleral multichannel electrode array in rabbit eyes. Graefes Arch Clin Exp Ophthalmol 2005;243:169–174
15. Fujikado T, Morimoto T, Kanda H, Kusaka S, Nakauchi K, Ozawa M, Matsushita K, Sakaguchi H, Ikuno Y, Kamei M, Tano Y. Evaluation of phosphenes elicited by extraocular stimulation in normals and by suprachoroidal-transretinal stimulation in patients with retinitis pigmentosa. Graefes Arch Clin Exp Ophthalmol 2007;245: 1411–1419
16. Santos A, Humayun MS, de Juan E Jr, Greenburg RJ, Marsh MJ, Klock IB, Milam AH. Preservation of the inner retina in retinitis pigmentosa. A morphometric analysis. Arch Ophthalmol 1997;115: 511–515
17. Sakaguchi H, Fujikado T, Kanda H, Osanai M, Fang X, Nakauchi K, Ikuno Y, Kamei M, Ohji M, Yagi T, Tano Y. Electrical stimulation with a needle-type electrode inserted into the optic nerve in rabbit eyes. Jpn J Ophthalmol 2004;48:552–557
18. Fang X, Sakaguchi H, Fujikado T, Osanai M, Kanda H, Ikuno Y, Kamei M, Ohji M, Gan D, Choi J, Yagi T, Tano Y. Direct stimulation of optic nerve by electrodes implanted in optic disc of rabbit eyes. Graefes Arch Clin Exp Ophthalmol 2005;243:49–56
19. Fang X, Sakaguchi H, Fujikado T, Osanai M, Ikuno Y, Kamei M, Ohji M, Yagi T, Tano Y. Electrophysiological and histological studies of chronically implanted intrapapillary microelectrodes in rabbit eyes. Graefes Arch Clin Exp Ophthalmol 2006;244: 364–375
20. Bishop PO, Kozak W, Vakkur GJ. Some quantitative aspects of the cat's eye: axis and plane of reference, visual field co-ordinates and optics. J Physiol 1962;163:466–502

Imaging of Titanium:Sapphire Laser Retinal Injury by Adaptive Optics Fundus Imaging and Fourier-Domain Optical Coherence Tomography

YOSHIYUKI KITAGUCHI, TAKASHI FUJIKADO, SHUNJI KUSAKA, TATSUO YAMAGUCHI, TOSHIFUMI MIHASHI, AND YASUO TANO

• PURPOSE: To examine and observe the subtle retinal injuries caused by a titanium:sapphire laser with a high-resolution adaptive optics (AO) fundus camera and with Fourier-domain optical coherence tomography (FD-OCT).
• DESIGN: Observational case series.
• METHODS: Four eyes of 2 individuals who experienced an accidental exposure to reflected light from a titanium: sapphire laser were examined. High-resolution retinal images were obtained with the AO fundus camera and by FD-OCT, and the images were compared with the findings obtained by standard clinical tests, including the Amsler test and fluorescein angiography (FA).
• RESULTS: The photoreceptor mosaic was absent in a localized area of the fovea in the images obtained by the AO fundus camera, and the photoreceptor outer segments (OS) were disrupted at the corresponding area in the FD-OCT images. The changes were detected not only in the symptomatic eye but also in the asymptomatic fellow eye in both patients. In 3 eyes, the geographic dark area in the AO image decreased during the follow-up examinations.
• CONCLUSIONS: Very small, localized photoreceptor disruptions can be detected in patients with minimal titanium:sapphire laser injury by cross-sectional imaging using OCT, but their extent was delineated more precisely by en face AO imaging. Because the area of the photoreceptor disruption is very small, especially in the nonsymptomatic fellow eye, it is strongly recommended that laser workers—even those without visual symptoms—be examined by FD-OCT, an AO camera, or both if they have not worn protective goggles while using a laser. (Am J Ophthalmol 2009;148:97–104. © 2009 by Elsevier Inc. All rights reserved.)

Accepted for publication Jan 21, 2009.
From the Department of Applied Visual Science, Osaka University Graduate School of Medicine (Y.K., T.F., S.K.); and the Department of Ophthalmology, Osaka University Graduate School of Medicine (Y.T.), Osaka, Japan; and the Topcon Research Institute (T.Y., T.M.), Tokyo, Japan.
Inquiries to Takashi Fujikado, Department of Applied Visual Science, Osaka University Graduate School of Medicine, 2-2 Yamadaoka, Suita, Osaka 565-0871, Japan; e-mail: fukikado@ophthal.med.osaka-u.ac.jp

ACCIDENTAL RETINAL LASER INJURIES ARE DIAGnosed when retinal damage is detected that is consistent with the visual deficits.[1] Intraretinal or subretinal hemorrhages, vitreous hemorrhages, macular edema, retinal pigmentation, and macular holes have been reported in many cases.[2] These alterations have been detected by conventional ophthalmoscopic examinations, including fluorescein angiography (FA) and optical coherence tomography (OCT). However, in cases of indirect exposure to scattered or reflected light or to long-duration exposures to a low-power laser beam, for example, a laser pointer, the retinal damage sometimes is undetectable by conventional ophthalmologic examinations despite the report of visual disturbances.[3]

With advances in retinal imaging, small focal changes in the retina can be detected. Fourier-domain OCT (FD-OCT) provides an axial resolution of approximately 3 μm compared with 10 μm with the standard OCT.[4–7] This resolution allows the identification of the external limiting membrane (first reflection line), the photoreceptor inner and outer segment junction (IS/OS; second line), the photoreceptor OS (between the second and third line), and the retinal pigment epithelium (RPE; fourth line).[4,7] This has enabled examiners to detect a lesion, for example, of the photoreceptor layer that cannot be detected by other examination methods. A disturbance of IS/OS junction has been reported in some retinal diseases, for example, postoperative retinal detachment, central serous chorioretinopathy, and retinal dystrophy, which cannot be seen ophthalmoscopically.[5,7,8–11] A macular microhole is difficult to detect ophthalmoscopically,[12] but can be detected reliably as a disruption of the outer retina or RPE layer by OCT[13] and as a disruption of the third line in the FD-OCT images.[14]

An adaptive optics (AO) fundus camera can obtain images with a transverse resolution of less than 2 μm, and the images of individual photoreceptors can be studied in living human eyes.[15–19] The origin of the high-reflectance cone mosaic in the AO fundus camera has been reported to be from both the IS/OS junction and the OS in normal retinas.[20] However, a recent study using AO-OCT reported that the cone mosaic was observed clearly at the level of the third bright line of the FD-OCT images, where the tips of the cone photoreceptor OS are enveloped by

0002-9394/09/$36.00
doi:10.1016/j.ajo.2009.01.019

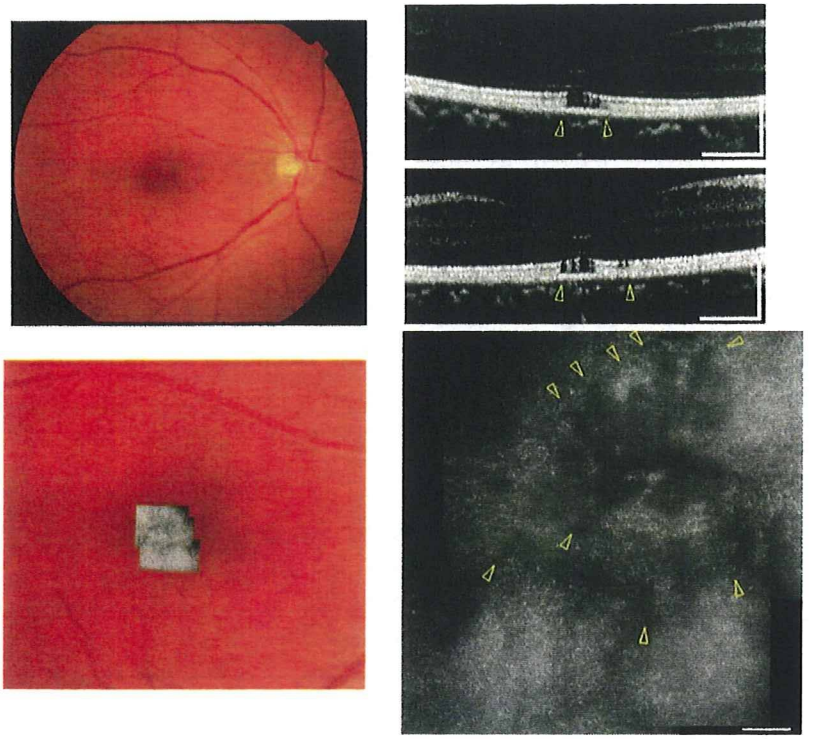

FIGURE 1. (Top left) Fundus photograph, (Top right [horizontal scan] and Middle right [vertical scan]) Fourier-domain optical coherence tomography (FD-OCT) images, and (Bottom left [low magnification] and Bottom right [high magnification]) adaptive optics (AO) images of the right eye of Patient 1 with titanium:sapphire retinal injury at the initial visit. The FD-OCT image shows a disruption of the photoreceptor inner segment and outer segment junction (IS/OS) and the OS (arrow head). The AO images show a geographic line-shaped dark area (arrowhead) above the fixation point. (Top right and Middle right) Horizontal bars represent 500 μm and vertical bars represent 200 μm. (Bottom right) Horizontal bar represents 100 μm.

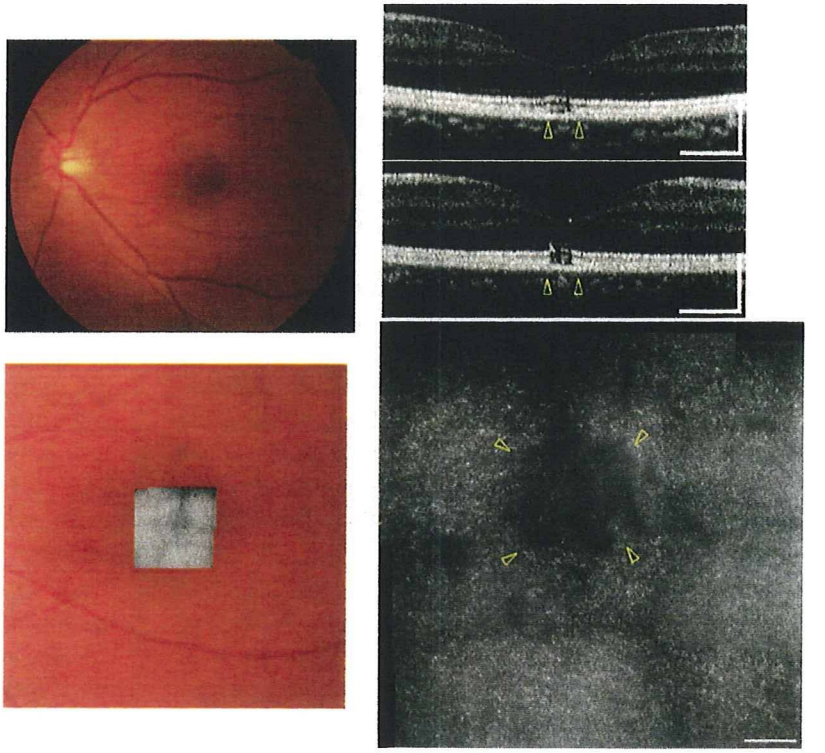

FIGURE 2. (Top left) Fundus photograph, (Top right [horizontal scan] and Middle right [vertical scan]) FD-OCT images, and (Bottom left [low magnification] and Bottom right [high magnification]) AO images of the left eye of Patient 1 with titanium:sapphire retinal injury at the initial visit. The FD-OCT image shows a disruption of the photoreceptor IS/OS and the OS (arrowhead). The AO images show a dark spotty area (arrowhead), and the area is smaller than that of right eye. (Top and Middle right) Horizontal bars represent 500 μm and vertical bars represent 200 μm. (Bottom right) Horizontal bar represents 100 μm.

the microvilli.[21] In our study of eyes with a macular microhole,[14] the OS may contribute more to the reflectance of the photoreceptor mosaic than the IS/OS junction in the AO images.

A reduction in the cone density in eyes with retinal dystrophy can be detected with an AO camera,[22,23] and a disruption of the third bright line of the FD-OCT images is reported to coincide with the dark areas in the AO camera images.[14]

Thus, the purpose of this study was to determine the cause of the visual disturbances reported by 2 patients who had worked with a titanium:sapphire laser. We show that the images obtained with the FD-OCT and AO both in depth and in the en face directions demonstrated retinal

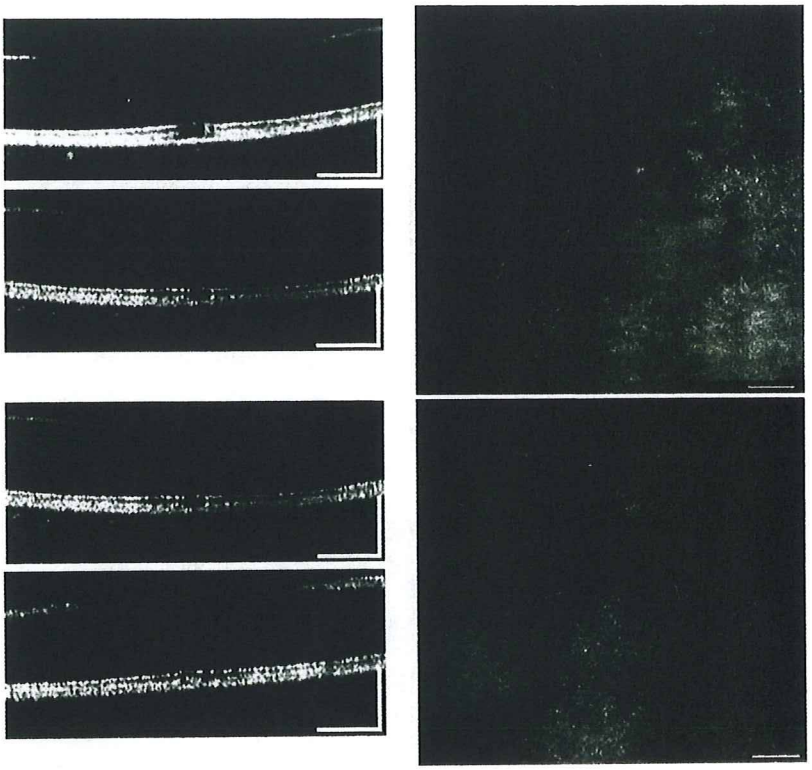

FIGURE 3. (Top left [horizontal scan] and second left [vertical scan]) FD-OCT images and (Top right) AO image of the right eye, and (Third left [horizontal scan] and Bottom left [vertical scan]) FD-OCT images (Bottom right) and AO image of the left eye of Patient 1 with titanium: sapphire retinal injury 6 months after the initial visit. The FD-OCT images are similar to that of the initial visit in both eyes. The AO image shows that the margin of line-shaped dark area is obscured in the right eye and that the dark spotty area has faded in the left eye. Horizontal bars in the left columns represent 500 μm, and vertical bars in the right columns represent 200 μm. Horizontal bar in the right column represents 100 μm. The arrowheads indicate the size of initial lesion.

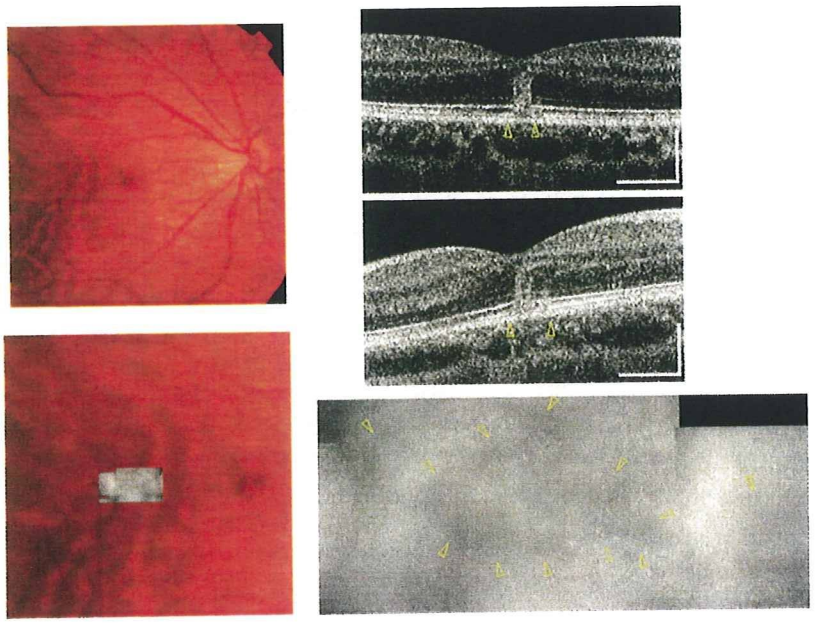

FIGURE 4. (Top Left) Fundus photograph, (Top right [horizontal scan] and Middle right [vertical scan]) FD-OCT images, and (Bottom left [low magnification] and Bottom right [high magnification]) AO images of the right eye of Patient 2 with titanium:sapphire retinal injury at the initial visit. FD-OCT image shows a penetrating lesion from the outer nuclear (ONL) layer to outer segment layer (OSL) in the fovea (arrowhead). The AO images show several spotty dark areas (arrowhead). (Top right and Middle right) Horizontal bars represent 500 μm and vertical bars represent 200 μm. (Bottom right) Horizontal bar represents 100 μm.

damage that was not visible by conventional ophthalmic instruments.

METHODS

• SUBJECTS: Two patients who reported visual disturbances after working with a titanium:sapphire laser beam were studied. The patients had visited the Osaka University Hospital between October 30, 2007 and June 13, 2008 and were followed up for more than 1 month. After the nature and possible consequences of the study were explained, written informed consent was obtained from the 2 patients.

• PROCEDURES: The 2 patients underwent a comprehensive ophthalmologic examination, including measurements of the best-corrected visual acuity (BCVA), Amsler chart testing, fundus photography, and slit-lamp biomicroscopy of the fundus. One patient underwent FA and the

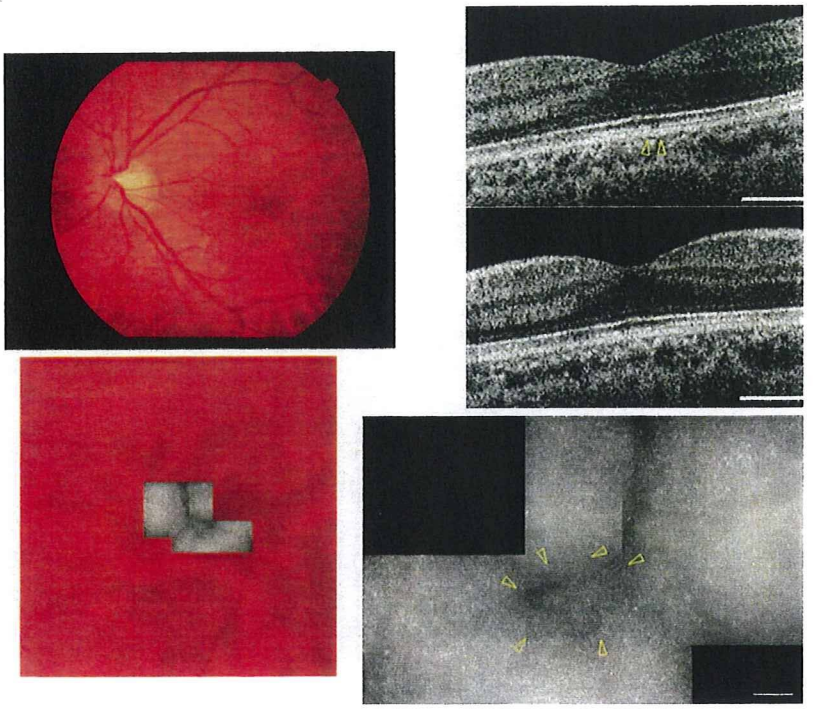

FIGURE 5. (Top left) Fundus photograph, (Top right [horizontal scan] and Middle right [vertical scan]) FD-OCT images, and (Bottom left [low magnification] and Bottom right [high magnification]) AO images of the left eye of Patient 2 with titanium:sapphire retinal injury at initial visit. The FD-OCT image shows a tiny OSL disturbance (arrowhead) on the horizontal scan. The AO images show a very small spotty dark area (arrowhead). (Top right and Middle right) Horizontal bars represent 500 μm and vertical bars represent 200 μm. (Bottom right) Horizontal bar represents 100 μm.

other underwent a fundus autofluorescence examination. They were also examined with the cube mode of FD-OCT (Cirrus OCT; Carl Zeiss Meditec, Dublin, California, USA) and a custom-built AO fundus camera.

A detailed description of the custom-built AO fundus camera has been published.[24,25] The principle of our flood-illumination AO fundus camera was similar to that reported by Roorda and Williams.[16] Briefly, the main components of the camera were a nematic liquid crystal phase modulator (X8267-12; Hamamatsu Photonics, Hamamatsu, Japan), a Hartmann-Shack wavefront sensor (28 × 28 lenslets, specially made by Topcon Co, Tokyo, Japan), and a scientific charge-coupled device digital camera (C9100-02; Hamamatsu Photonics). The wavefront sensor measured the ocular wavefront up to the eighth Zernike order, and the phase modulator compensated for the measured wavefront aberrations. The light source for the imaging was a laser diode (LLS-635-50; Moritex, Tokyo, Japan) with a wavelength of 635 nm. Because the light source was coherent, the images we obtained were different from those of an earlier study in which the light source was noncoherent.[16] The system also was equipped with coaxial, 8-degree wide viewing optics to identify the location and orientation of the highly magnified retinal images being examined.

Topical tropicamide (0.5%) and phenylephrine (0.5%) were used to dilate the pupil and to paralyze the ciliary muscle. The retina was illuminated by a laser diode (635-nm wavelength), and a retinal image was obtained with a shutter of 2 milliseconds with a 6-mm diameter exit pupil. The patient was instructed to fixate on a designated position on a target. Overlapping images were merged using Photoshop (Adobe Systems Inc, San Jose, California, USA). To identify the fovea, a montage of the AO images was made and superimposed on the fundus photographs and on the fundus projection of the OCT images.

• PATIENT 1: A 44-year-old male optical engineer who worked with a titanium:sapphire laser (pulse mode; wavelength, 400 nm and 800 nm; frequency, 1 kHz; duration, 100 femtosecond; power, 1 mJ) reported visual disturbances in his right eye. He had been working with the laser without goggles, but had not had a direct exposure to the laser beam. His BCVA was 20/50 in the right eye and 20/20 in the left eye. The fundus of both eyes appeared to be normal ophthalmoscopically (Figures 1 and 2, Top left). A relative scotoma was identified below the fixation point by the Amsler test in the right eye. The retinal autofluorescence image was normal in both eyes.

Fourier-domain OCT demonstrated a disruption of the IS/OS line and the OS layer of approximately 300 μm on the horizontal scan and 500 μm on the vertical scan of his right eye (Figure 1, Top right and Middle right). The external limiting membrane and RPE layer were intact. Interestingly, there was also a 200 × 200-μm disruption of the OS layer in his left eye (Figure 2, Top right and Middle right).

The AO image showed a very small dark area, that is, an absence of the cone mosaic, at the fovea just above the fixation point in both eyes. The shape of dark area was geographic, several line-shaped dark areas extended radially in the right eye, and a round dark area in the left eye was present (Figures 1 and 2, Bottom right). The area was larger in the right eye than in the left eye. The horizontal

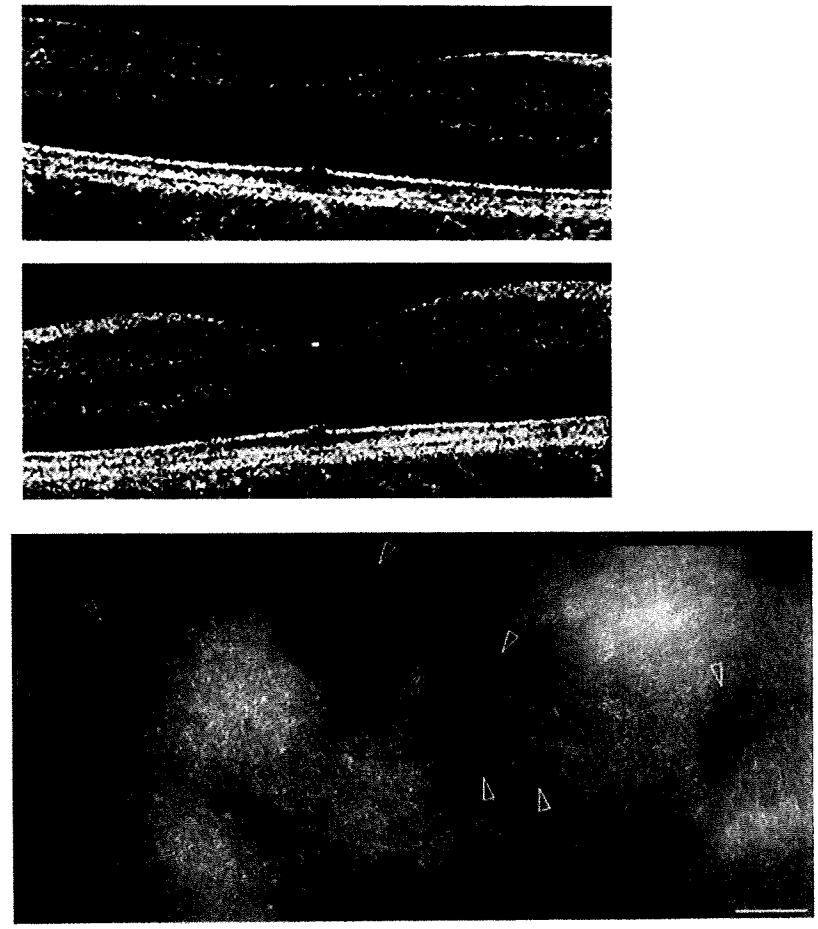

FIGURE 6. (Top [horizontal scan] and Middle [vertical scan]) FD-OCT image and (Bottom) AO image of the right eye of Patient 2 with titanium:sapphire retinal injury obtained 1 month after the initial visit. The FD-OCT image shows an almost intact ONL, and the size of disruption of the photoreceptor IS/OS junction and OS layer (arrowhead) is less than that at the initial visit. The AO images show that the area of the dark spots (arrowhead) also is reduced. (Top and Middle) Horizontal bars represent 500 μm and vertical bars represent 200 μm. (Bottom) Horizontal bar represents 100 μm.

and vertical sizes of the dark areas were 300 × 500 μm in the right eye and 200 × 200 μm in the left eye, and these sizes were comparable with those of the FD-OCT images of both eyes.

Six months after the first visit, his symptoms, the visual acuity (VA), and the area of IS/OS disruption in the FD-OCT (Figure 3, Top left, Second left, Third left, and Fourth left) had not changed in both eyes, but the margin of the line-shaped dark areas in the AO image was not well defined in the right eye, and the round dark area had faded in the left eye (Figure 3, Top right and Bottom right). The patient had not worked with the laser during this period.

• PATIENT 2: A 24-year-old male graduate student who worked in a chemistry laboratory using a titanium:sapphire laser (780 nm, 200-mW pulse mode). He had worked with a laser without wearing goggles and accidentally stared at the reflected laser beam from the wall of a cell during the alignment procedures the day before the first visit. He reported blurred vision in his right eye.

His BCVA was 20/25 in the right eye and 20/20 in the left eye. His fundus appeared to be normal without edema or retinal hemorrhage ophthalmoscopically (Figure 4, Top left). Amsler chart examination showed a localized relative scotoma around the fixation point. FA results were normal in both eyes.

Fourier-domain OCT demonstrated a penetrating lesion from the outer nuclear layer (ONL) to the OS layer in the fovea of the right eye (Figure 4, Top and Middle right). The area of disturbance in the IS/OS junction was approximately 200 μm on the horizontal scan and 300 μm on the vertical scan. There was a small OS layer disturbance (100 μm on the horizontal scan) in his left eye (Figure 5, Top right).

The AO image showed several spotty dark areas in the right eye ranging from approximately 800 μm horizontally and 400 μm vertically and a very small spot in the left eye (400 × 400 μm; Figures 4 and 5, Bottom right). The horizontal and vertical sizes of the dark area in the AO image were larger than the IS/OS or OS disturbances in those of FD-OCT scan in both eyes.

One month after the first visit, the subjective symptoms improved in the right eye and the area of relative scotoma was reduced in the Amsler chart. The VA in the right eye improved to 20/20. The penetrating lesion in the ONL in the FD-OCT scan could not be detected, and the size of the disruption of the IS/OS junction and the OS layers was reduced in the right eye (Figure 6, Top and Middle). The

area of the dark spots in the AO images was also reduced (Figure 6, Bottom).

RESULTS

BOTH OF THE PATIENTS EXPERIENCED AN EXPOSURE TO reflected light from a pulsed titanium:sapphire laser. Patient 1 did not note the bright reflected light, but Patient 2 looked at the bright reflected light. The fundus photographs had normal results in both eyes of both patients. The retinal autofluorescence image showed normal results in Patient 1, and the FA results were normal in Patient 2, which suggested that the disturbances of the RPE were negligible in both cases.

In the FD-OCT scans, the horizontal and vertical sizes of the disturbances in the IS/OS and OS layers were very restricted in both patients, and they coincided with the dark area of the AO image in both eyes of Patient 1, but were smaller than the dark area in the AO image of the right eye of Patient 2. The disturbances in the photoreceptors in the FD-OCT or AO images were observed not only in the symptomatic eye but also in the asymptomatic fellow eye in both patients.

In the right eye of Patient 1, the shape of dark area in AO had a geographic pattern in which several line-shaped dark areas were gathered radially, suggesting that the subclinical retinal injuries had been accumulating. During the follow-up, the margin of the dark areas in the AO image was obscured in Patient 1, and the penetrating injury in the nuclear layer disappeared with a reduction in the size of the IS/OS disruption in FD-OCT images and with a reduction of the area of dark spots in AO images in Patient 2.

DISCUSSION

THESE RESULTS INDICATE THAT MINIMAL RETINAL LASER damages, which are difficult or even impossible to detect with conventional ophthalmologic instruments, can be detected clearly by FD-OCT in depth or with an AO fundus camera in the en face direction. The AO camera enables an examination of the lateral extent of the defect, whereas the FD-OCT allows a cross-sectional examination of the photoreceptor disturbances in vivo. We have reported that disturbances of the photoreceptor layer in eyes with a macular microhole were imaged clearly by FD-OCT and the lateral extent of the lesion could be detected by a flood-illumination AO camera.[14]

The localized photoreceptor disruption caused by reflected light from the titanium:sapphire laser was identified by FD-OCT and AO imaging. To the best of our knowledge, this is the first report of selective photoreceptor damage resulting from titanium:sapphire laser that was identified and observed using FD-OCT and AO.

The photoreceptor damages detected in the OCT or AO images are reportedly related to visual disfunction in some retinal diseases.[5,26–28] Ojima and associates used microperimetry in eyes with resolved central serous chorioretinopathy and showed focal areas with reduced retinal function. These areas corresponded with a defect of the IS/OS line or irregularity of the RPE layer.[28] Choi and associates and Duncan and associates reported a decrease in cone density measured with an AO fundus camera and showed that the cone density was correlated with the amplitude of the multifocal electroretinogram.[23,29] In our patients, a disruption of the foveal photoreceptors observed in the FD-OCT and AO images were consistent with the relative scotoma in the Amsler test in the more affected eyes.

The AO image showed that the area of photoreceptor disruption was not round, but rather geographic (Figure 1, Bottom right). The complicated pattern of the area of photoreceptor loss may not be reconstructed from the data of the current FD-OCT, so the en face AO image was useful in evaluating the 2-dimensional area of the photoreceptor damage.

In the right eye of Patient 2, a lesion that extended from the inner retina to the outer retina was detected by FD-OCT. The horizontal size of the lesion was approximately 200 μm (approximately 1.0 degree), which was much smaller than the visual angle of metamorphopsia measured by the Amsler test (oval shape with 8 × 4 degrees). The visual angle of the metamorphopsia corresponded to the area of photoreceptor disruption measured by the AO fundus image. This discrepancy may be because the interval of the horizontal scan was 50 μm by FD-OCT and the maximal extent of the lesion could not be measured precisely.

In the 1-month follow-up of the right eye of Patient 2, the vision recovered to some extent with the disappearance of penetrating lesion in the ONL in the FD-OCT image and a fading of the dark areas in the AO image. The exact mechanism that led to the visual recovery is not clear, but the imaging data suggest that a reorganization of the photoreceptor cells might have occurred after the acute stages of foveal injury. Even in Patient 1, whose vision did not recover, the margin of the line-shaped dark geographic area in the AO image was obscured during the follow-up. Because the patient did not carry out laser experiments during this period, a reorganization of photoreceptor cells also might have occurred. Such reorganization may imply either a lateral displacement of adjacent photoreceptors or a regeneration of the OS of the same photoreceptors.

Fluorescein angiography or autofluorescence imaging demonstrated that the RPE was not damaged in the 2 patients. The reported cases of retinal injury by neodymium:yttrium–aluminum–garnet or titanium:sapphire laser were more severe, and a macular hole developed accompanied by changes in the RPE.[30–34] The pulse

duration of the titanium:sapphire laser is very short, in fact, hundreds of femtoseconds, so the mechanical effect of shock waves predominates over the thermal effect. Both of the patients received indirect reflected light from the laser, so the energy to the retina was less than the direct exposure to the laser beam. These factors may explain why the damages were confined to the photoreceptor layer.

In both patients, a disruption of the photoreceptors caused by reflected light from the laser was detected in both eyes by FD-OCT and with the AO fundus camera, although they had no visual symptoms in their less-affected fellow eye and no abnormal findings were detected with conventional ophthalmologic examinations. It has been reported that 8% of laser injuries are binocular.[2] These findings suggest that there may be more binocular cases than reported, and these can be detected best by FD-OCT or with the AO fundus camera.

Patient 1 did not have a direct exposure of the laser beam, but based on the pattern of the dark area in the image obtained by the AO fundus camera, we suggest that repeated indirect exposures by scattered and reflected laser light might have a cumulative effect on the retina. Although no symptoms were observed in his left eye, visual disturbances may appear in the future if the patient continues working without goggles and experiences repeated minimal exposures to the retinas.

Both of our patients did not wear goggles when they were working with the laser. Wearing protective goggles is required by law in many countries; however, many workers work without goggles because wearing goggles reduces the field of vision and the light intensity.[35] We suggest that others who work with lasers also may have retinal laser injury that can be detected only by FD-OCT or by the AO fundus camera, even those without visual symptoms. Therefore, it may be necessary to examine the eyes of optical engineers who have been involved in experiments with a laser without wearing goggles, even if they do not have visual symptoms. The ability of FD-OCT or AO fundus camera to detect a very restricted lesion in the fovea also may be applicable to other sources or forms of photic injury.

Two limitations of this study are the small number of patients and the short follow-up. Future studies with larger numbers of patients may be helpful to determine whether photoreceptor damage and inner retinal damage will be repaired in the natural course of the recovery process. Another limitation is the resolution limit of cone photoreceptors in the fovea. The AO fundus camera had a transverse resolution of less than 2 μm,[15] but the photoreceptors in the fovea are smaller than this resolution limit. Thus, it is difficult to evaluate quantitatively the disturbance of photoreceptor cells in the center of the fovea.

In conclusion, extremely localized photoreceptor disruptions can be detected in patients with minimal titanium: sapphire laser injury by FD-OCT in the depth direction and by AO imaging in the en face direction. The geographic dark area in the AO images in Patient 1 suggests that the subclinical laser damage is cumulative and eventually leads to visual symptoms. Because a very small area of photoreceptor disruption was observed even in the nonsymptomatic fellow eye in both patients, it is strongly recommended that laser workers or researchers even without visual symptoms be checked by FD-OCT, an AO fundus camera, or both if they have not worn protective goggles.

THIS STUDY WAS SUPPORTED BY HEALTH SCIENCES RESEARCH GRANTS NO. H19-SENSORY-001 FROM THE MINISTRY OF Health, Labor and Welfare, Tokyo, Japan. Drs Yamaguchi and Mihashi are employees of Topcon Co. Involved in design of study (T.F., S.K.); conduct of study (Y.K., T.Y.); analysis and interpretation of data (Y.K., T.F.); writing the article (Y.K., T.F.); critical revision of the article (T.M., Y.T.); and preparation, review, and approval of the manuscript (S.K.). The research protocol was approved by the Institutional Review Board of the Osaka University Medical School. The procedures performed conformed to the tenets of the Declaration of Helsinki.

REFERENCES

1. Mainster MA, Stuck BE, Brown J Jr. Assessment of alleged retinal laser injuries. Arch Ophthalmol 2004;122:1210–1217.
2. Barkana Y, Belkin M. Laser eye injuries. Surv Ophthalmol 2000;44:459–478.
3. Sethi CS, Grey RH, Hart CD. Laser pointers revisited: a survey of 14 patients attending casualty at the Bristol Eye Hospital. Br J Ophthalmol 1999;83:1164–1167.
4. Drexler W, Sattmann H, Hermann B, et al. Enhanced visualization of macular pathology with the use of ultra-high resolution optical coherence tomography. Arch Ophthalmol 2003;121:695–706.
5. Schocket LS, Witkin AJ, Fujimoto JG, et al. Ultra-high resolution optical coherence tomography in patients with decreased visual acuity after retinal detachment repair. Ophthalmology 2006;113:666–672.
6. Alam S, Zawadzki RJ, Choi S, et al. Clinical application of rapid serial Fourier-domain optical coherence tomography for macular imaging. Ophthalmology 2006;113:1425–1431.
7. Ojima Y, Hangai M, Sasahara M, et al. Three-dimensional imaging of the foveal photoreceptor layer in central serous chorioretinopathy using high-speed optical coherence tomography. Ophthalmology 2007;114:2197–2207.
8. Ergun E, Hermann B, Wirtitsch M, et al. Assessment of central visual function in Stargardt disease/fundus flavimaculatus with ultra-high resolution optical coherence tomography. Invest Ophthalmol Vis Sci 2005;46:310–316.
9. Wirtitsch MG, Ergun E, Hermann B, et al. Ultra-high resolution optical coherence tomography in macular dystrophy. Am J Ophthalmol 2005;140:976–983.
10. Piccolino FC, Longrais RR, Ravera G, et al. The foveal photoreceptor layer and visual acuity loss in central serous chorioretinopathy. Am J Ophthalmol 2005;139:87–99.

11. Iida T, Hagimura N, Sato T, et al. Evaluation of central serous chorioretinopathy with optical coherence tomography. Am J Ophthalmol 2000;129:16–20.
12. Cairns JD, McCombe MF. Microholes of the fovea centralis. Aust N Z J Ophthalmol 1988;16:75–79.
13. Zambarakji HJ, Schlottmann P, Tanner V, et al. Macular microholes: pathogenesis and natural history. Br J Ophthalmol 2005;89:189–193.
14. Kitaguchi Y, Fujikado T, Bessho K, et al. Adaptive optics fundus camera to examine localized changes in the photoreceptor layer of the fovea. Ophthalmology 2008;115:1771–1777.
15. Liang J, Williams DR, Miller DT. Supernormal vision and high resolution retinal imaging through adaptive optics. J Opt Soc Am A Opt Image Sci Vis 1997;14:2884–2892.
16. Roorda A, Williams DR. The arrangement of three cone classes in the living human eye. Nature 1999;397:520–522.
17. Roorda A, Williams DR. Optical fiber properties of individual human cones. J Vis 2002;2:404–412.
18. Roorda A, Romero BF, Donnelly WJ, et al. Adaptive optics scanning laser ophthalmoscopy. Opt Express 2002;10:405–412.
19. Pallikaris A, Williams DR, Hofer H, et al. The reflectance of single cones in the living human eye. Invest Ophthalmol Vis Sci 2003;44:4580–4592.
20. Pircher M, Baumann B, Gotzinger E, Hitzenberger CK. Retinal cone mosaic imaged with transverse scanning optical coherence tomography Optics Lett 2006;31:1821–1823.
21. Zawadzki RJ, Choi SS, Jones SM, et al. Adaptive optics-optical coherence tomography: optimizing visualization of microscopic retinal structures in three dimensions. J Opt Soc Am A Opt Image Sci Vis 2007;24:1373–1383.
22. Wolfing JI, Chung M, Carrol J, et al. High-resolution retinal imaging of cone-rod dystrophy. Ophthalmology 2006;113:1014–1019.
23. Choi SS, Doble N, Hardy JL, et al. In vivo imaging of the photoreceptor mosaic in retinal dystrophies and correlations with visual function. Invest Ophthalmol Vis Sci 2006;47:2080–2092.
24. Kitaguchi Y, Bessho K, Yamaguchi T, et al. In vivo measurements of cone photoreceptor spacing in myopic eyes from images obtained by adaptive optics fundus camera. Jpn J Ophthalmol 2007;51:456–461.
25. Yamaguchi T, Nakazawa N, Bessho K, et al. Adaptive optics fundus camera using a liquid crystal phase modulator. Opt Rev 2008;15:173–180.
26. Ergun E, Hermann B, Wirtitsch M, et al. Assessment of central visual function in Stargardt disease/fundus flavimaculatus with ultra-high resolution optical coherence tomography. Invest Ophthalmol Vis Sci 2005;46:310–316.
27. Piccolino FC, Longrais RR, Ravera G, et al. The foveal photoreceptor layer and visual acuity loss in central serous chorioretinopathy. Am J Ophthalmol 2005;139:87–99.
28. Ojima Y, Tsujikawa A, Hangai M, et al. Retinal sensitivity measured with the micro perimeter 1 after resolution of central serous chorioretinopathy. Am J Ophthalmol 2008;146:77–84.
29. Duncan JL, Zhang Y, Gandhi J, et al. High-resolution imaging with adaptive optics in patients with inherited retinal degeneration. Invest Ophthalmol Vis Sci 2007;48:3283–3291.
30. Sasahara M, Noami S, Takahashi M, et al. Optical coherence tomographic observations before and after macular hole formation secondary to laser injury. Am J Ophthalmol 2003;136:1167–1170.
31. Nehemy M, Torqueti-Costa L, Magalhães EP, et al. Choroidal neovascularization after accidental macular damage by laser. Clin Exp Ophthalmol 2005;33:298–300.
32. Newman DK, Flanagan DW. Spontaneous closure of a macular hole secondary to an accidental laser injury. Br J Ophthalmol 2000;84:1075.
33. Sakaguchi H, Ohji M, Kubota A, et al. Amsler grid examination and optical coherence tomography of a macular hole caused by accidental Nd:YAG laser injury. Am J Ophthalmol 2000;130:355–356.
34. Sou R, Kusaka S, Ohji M, et al. Optical coherence tomographic evaluation of a surgically treated traumatic macular hole secondary to Nd:YAG laser injury. Am J Ophthalmol 2003;135:537–539.
35. Kamijo Y, Ozawa T. Accidental laser eye in Japan [in Japanese]. Jpn Rev Clin Ophthalmol 2003;97:95–100.

Generation of a Transgenic Rabbit Model of Retinal Degeneration

Mineo Kondo,[1] *Takao Sakai,*[1] *Keiichi Komeima,*[1] *Yukihide Kurimoto,*[1] *Shinji Ueno,*[1] *Yuji Nishizawa,*[2] *Jiro Usukura,*[3] *Takashi Fujikado,*[4] *Yasuo Tano,*[5] *and Hiroko Terasaki*[1]

Purpose. To generate a transgenic (Tg) rabbit model of retinal degeneration and to characterize the pattern of degeneration by using histology and electrophysiology.

Methods. Rhodopsin Pro347Leu Tg rabbits were generated by BAC transgenesis. Tg rabbits were identified by Southern blot analysis, and the expression levels were measured by quantitative RT-PCR. Retinal histology was examined by light and electron microscopy and immunohistochemistry. Retinal function was assessed by full-field electroretinograms (ERGs).

Results. Six lines of Tg rabbits were generated, and two lines with higher levels of expression showed rod-dominant progressive retinal degeneration. Retinal histology indicated a marked regional variation in the loss of photoreceptors with the central retina more severely affected than the peripheral retina. The characteristics of the ERGs of transgenic rabbits indicated that the rod components of the ERGs were reduced to only 5% by 48 weeks, whereas the cone components remained at 35% in the wild-type at the same time point. The retinal ultrastructure of Tg rabbits showed a large number of small vesicles that accumulated in the extracellular space of the photoreceptors.

Conclusions. To the best of the authors' knowledge, this is the first rabbit model of progressive retinal degeneration. Because rabbits have large eyes and are easy to handle and breed, they will provide a useful animal model for the study of the pathophysiology of and new treatments for retinal degeneration. (*Invest Ophthalmol Vis Sci.* 2009;50:1371-1377) DOI:10.1167/iovs.08-2863

Retinitis pigmentosa (RP) is the name given to a group of inherited retinal disorders characterized by a progressive loss of rod and cone photoreceptors and eventual atrophy of the entire retina.[1-3] The worldwide prevalence of RP is approximately 1 in 4000, meaning that more than 1 million individuals are affected worldwide.[3] RP is genetically heterogeneous; mutations in several photoreceptor-specific and some nonspecific genes are known to cause the condition.[4] Of these, mutations in the rhodopsin gene are the most prevalent class identified to date, causing approximately 25% to 40% of the autosomal dominant RP cases.[5,6]

Animal models of RP are important for understanding the pathophysiology and for developing new treatments for these diseases. Various naturally occurring and genetically manipulated animal models of RP have been studied—for example, fruit flies, zebrafish, chickens, mice, rats, cats, dogs, and pigs (for reviews, see Refs. 7, 8). Of these models, midsized and large animal models have become particularly important because their large eyes make it easier to test new treatments. These treatments may include surgical procedures such as intraocular devices,[9,10] subretinal injection of genes for gene therapy,[11] and implantation of retinal prostheses.[12] Several models of retinal degeneration have been identified or generated in cats,[13,14] dogs,[15,16] and pigs,[17] and colonies of affected animals have been established. However, a rabbit model of progressive retinal degeneration has not yet been produced, despite the fact that this animal has large eyes and is easy to breed and handle. In addition, there is a considerable accumulation of past works on the anatomy and physiology of the rabbit eye.[18-21]

Recent advances in the use of bacterial artificial chromosomes (BACs) modified by homologous recombination have promoted the use of this powerful tool in the generation of transgenic (Tg) animals because this technique makes possible the precise and efficient engineering of large DNA fragments.[22-25] In the present study, we used BAC transgenesis to generate a rhodopsin Tg rabbit model of retinal degeneration. These Tg rabbits exhibited rod-dominant, progressive photoreceptor degeneration and striking regional variation in the pattern of photoreceptor loss.

Methods

This study was conducted in accordance with the ARVO Statement for the Use of Animals in Ophthalmic and Vision Research. All protocols were approved by the Institutional Review Board of the Nagoya University Graduate School of Medicine.

Rabbit Rhodopsin BAC Clone

The rabbit rhodopsin BAC clone, LB1-7M22, was selected from the LBNL-1 New Zealand White Rabbit BAC library by hybridization of high-density arrayed nylon filters using a probe that consisted of a [P^{32}]-labeled fragment of exon 5 of the rabbit rhodopsin gene. The clone was obtained from the BACPAC Resources Center at the Children's Hospital of Oakland Research Institute. The presence of a full-length rabbit rhodopsin genomic sequence was verified by Southern blot analysis with a probe that consisted not only of exon 4 of the rhodopsin gene but also exon 14 of the rabbit *WDR10* gene and exon 25 of the rabbit *PLXND1* gene. These latter two genes are the 5′- and 3′-flanking genes, respectively, of the rabbit rhodopsin gene (Fig. 1A). The exon 4 genomic fragment of the rabbit rhodopsin gene, exon 14

From the [1]Department of Ophthalmology, Graduate School of Medicine, and the [3]Department of Materials Physics and Engineering, Graduate School of Engineering, Nagoya University, Nagoya, Japan; the [2]Research Institute of Life and Health Sciences, Chubu University, Kasugai, Japan; and the Departments of [4]Applied Visual Science and [5]Ophthalmology, Graduate School of Medicine, Osaka University, Suita, Japan.

Supported by Health Sciences Research Grant H16-sensory-001 from the Ministry of Health, Labor, and Welfare of Japan, and Grants 18591913 and 18390466 from the Ministry of Education, Culture, Science, and Technology of Japan.

Submitted for publication September 12, 2008; revised November 9, 2008; accepted January 2, 2009.

Disclosure: **M. Kondo**, None; **T. Sakai**, None; **K. Komeima**, None; **Y. Kurimoto**, None; **S. Ueno**, None; **Y. Nishizawa**, None; **J. Usukura**, None; **T. Fujikado**, None; **Y. Tano**, None; **H. Terasaki**, None

The publication costs of this article were defrayed in part by page charge payment. This article must therefore be marked "*advertisement*" in accordance with 18 U.S.C. §1734 solely to indicate this fact.

Corresponding author: Mineo Kondo, Department of Ophthalmology, Nagoya University Graduate School of Medicine, 65 Tsuruma-cho, Showa-ku, Nagoya 466-8550, Japan; kondomi@med.nagoya-u.ac.jp.

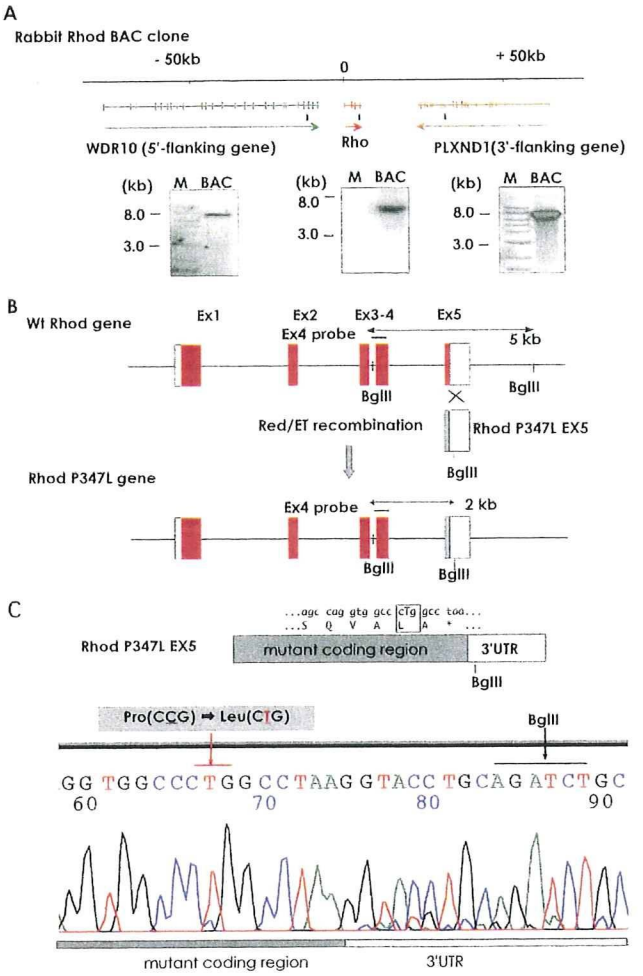

FIGURE 1. Rhodopsin P347L BAC construction by recombineering. (**A**) Presumed structure of the rabbit rhodopsin BAC clone. The BAC clone contains the full-length rabbit rhodopsin genomic sequence, as determined by Southern hybridization probed by the 5′-flanking gene (*left*), rhodopsin gene (*middle*), and 3′-flanking gene (*right*). *Underbars*: positions of the Southern hybridization probes used. (**B**) The transgene construct. The sequence of exon 5 of the WT rhodopsin gene (*top*) was replaced by the rhodopsin P347L exon 5 sequence (*middle*) by Red/ET recombination. The rhodopsin P347L gene (*bottom*) has a *Bgl*II restriction site for Tg. (**C**) Sequence analysis for the rhodopsin P347L mutation. The rhodopsin P347L exon 5 fragment was amplified from the rhodopsin P347L BAC construct by PCR and sequenced.

of the rabbit *WDR10* gene, and exon 25 of the rabbit *PLXND1* gene were amplified by PCR and subcloned into the pGEM-T easy vector (Promega, Madison, WI) for labeling with [P^{32}].

BAC Tg Construct

A rhodopsin P347L BAC Tg construct harboring a C-to-T transition in exon 5 of the rabbit rhodopsin gene was generated by BAC recombineering (Fig. 1B). A point mutation was introduced into the rabbit rhodopsin BAC clone.[24] In brief, an rpsL-neo counter selection cassette, flanked by 40-nucleotide homologous arm sequences on either side of the C-to-T transition site of the rhodopsin gene, was amplified by PCR. The amplified rpsL-neo counter selection cassette was inserted into the rhodopsin gene of the rabbit BAC clone by Red/ET recombination. The subcloned exon 5 fragment of the rabbit rhodopsin gene was modified with a C-to-T transition at proline 347, and the serial restriction sites *Kpn*I, *Pst*I, and *Bgl*II in the 3′-untranslated region. The modified sequence was subcloned into the pGEM-T easy vector for sequencing. The rpsL-neo cassette inserted into the rhodopsin gene of the rabbit BAC clone was replaced by the modified exon 5 fragment by using rpsL counter selection. The BAC modification was verified by Southern blot analysis and sequencing (Fig. 1C). The rhodopsin P347L BAC transgene was purified in a modified procedure.[26] The BAC Tg construct was extracted from 250 mL of *Escherichia coli* culture. For purification, 10 μg of the BAC Tg construct was linearized overnight with PI-*Sce*I endonuclease (New England Biolabs, Beverly, MA), which cleaves a unique site in the BACe3.6 vector sequence. The linearized BAC DNA was separated by pulsed-field gel electrophoresis (PFGE) and extracted from the preparative pulsed-field gel by electroelution. After dialysis against a TE buffer containing 0.1 mM EDTA, aliquots of DNA were subjected to PFGE for size and quality control. The BAC DNA concentration was adjusted to 1 ng/μL for microinjections. The aliquots of BAC DNA solution were stored at 4°C until the microinjections were performed.

Rhodopsin P347L Tg Rabbits

Rhodopsin P347L Tg rabbits were generated by pronuclear injection of the BAC Tg construct into New Zealand White rabbit embryos. Transgenic founders and germline transmission of the BAC Tg construct were assessed by Southern blot analysis of *Bgl*II-digested ear DNA, which was probed with a [P^{32}]-labeled exon 4 fragment of the rabbit rhodopsin gene.

DNA Fluorescence In Situ Hybridization Analysis

DNA FISH analysis was used to examine the actual site of the integrated transgene for each Tg line. Chromosome preparations were obtained with standard techniques and hybridized with a full-length rhodopsin P347L BAC Tg construct as a probe. The probe was labeled with biotin (Roche Diagnostics GmbH, Mannheim, Germany) and detected with avidin-FITC (Fluorescein Avidin D; Vector Labs, Burlingame, CA). The site of the transgene integration was determined by using a standard rabbit chromosome map.[27]

Quantitative RT-PCR

One milligram of total retinal RNA (12 weeks of age) was incubated with 200 units of reverse transcriptase (SuperScript II; Invitrogen, Carlsbad, CA), and the cDNA was used for quantitative RT-PCR (qRT-PCR; QuantiTect SYBR Green PCR Kit; Qiagen, Valencia, CA) and a thermocycler (LightCycler 1.5; Roche Applied Science, Indianapolis, IN). Twenty-microliter reactions were loaded into the thermocycler containing 2 μL of the cDNA sample and 0.5 μM of primers specific for the mutated rhodopsin (forward: 5′-CTA CAT CAT GAT GAA CAA GCA G-3′ and reverse: 5′-TGG CTG GTC TCC GTC TTG GAA-3′) or common primers for wild-type (WT) and mutated rhodopsin (forward: 5′-CTA CAT CAT GAT GAA CAA GCA G-3′ and reverse: 5′-GCA GTG CAG ATC TGC AGG T-3′). For quantification, a standard curve was generated from a cDNA template for each gene. The relative levels of transgene expression were quantified as a ratio of the Tg to the endogenous rhodopsin mRNA.

Clinical Ophthalmic Observations

Ophthalmic examinations were conducted every month after birth. Examinations of the cornea, anterior chamber, iris, and lens were performed by slit-lamp biomicroscopy. The vitreous and retina were examined by indirect ophthalmoscopy. A fundus camera (Kowa, Nagoya, Japan) was used for fundus photography and fluorescein angiography.

Electroretinograms

Animals were dark-adapted for 60 minutes, then anesthetized with ketamine (25 mg/kg, IM) and xylazine (2 mg/kg, IM). ERGs were recorded with Burian-Allen bipolar contact lens electrodes (Hansen Laboratory, Iowa City, IA). The animals were placed in a Ganzfeld bowl and stimulated with stroboscopic stimuli of 2.2 log cd · s · m^{-2}

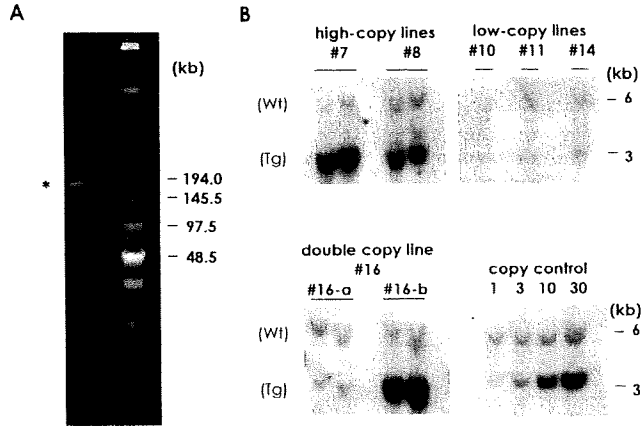

FIGURE 2. Generation of rhodopsin P347L Tg rabbits. (A) Purified rhodopsin P347L transgene construct. PFGE showed that the purified rhodopsin P347L transgene construct was almost 150 kb in size. (B) Southern blot analysis of F1 rabbits of rhodopsin P347L Tg lines. The endogenous rhodopsin WT gene and the rhodopsin P347L transgene were detected as 6 and 3 kb *Bgl*II fragments that hybridized to an exon 4 probe. The copy numbers of the integrated transgene for each line were determined by comparing with a control copy number signal intensity.

(photopic units) maximum intensity. Eight steps of stimulus intensities, ranging from −4.8 to 2.2 log cd · s · m^{-2}, were used for the scotopic ERG recordings, and four steps of stimuli, ranging from −0.8 to 2.2 log cd · s · m^{-2}, were used for the photopic ERGs. The photopic ERGs were recorded on a rod-suppressing white background of 1.3 log cd · m^{-2}. The signals were amplified, bandpass filtered between 0.3 and 1000 Hz, and averaged by a computer-assisted signal analysis system (MEB-9100 Neuropack; Nihon Kohden, Tokyo, Japan). The electrical activities of the rod and cone photoreceptors were assessed by the maximum response of the rod and cone a-waves. The maximum rod a-wave was extracted by waveform subtraction of the photopic ERG from the scotopic ERG at the maximum stimulus intensity of 2.2 log cd · s · m^{-2}.

Rod and cone photoreceptor function was also assessed by the a-wave (P3)-fitting model of Hood and Birch.[28] The a-wave was fitted with the following equation:

$$P3(i, t) = \{1 - \exp[-i \cdot S(t - t_d)^2]\} \cdot Rm \text{ (for } t > t_d)$$

where i is the flash energy (log cd · s · m^{-2}); t_d is the time delay, t is the time after the flash onset, S is the sensitivity, and Rm is maximum response amplitude.

Retinal Histology

Rabbit eyes were fixed overnight in a mixture of 10% neutral buffered formalin and 2.5% glutaraldehyde; F-G fixative), then transferred to 10% neutral buffered formalin. The tissues were trimmed, embedded in paraffin, sectioned vertically through the optic nerve (superior-inferior), and stained with hematoxylin and eosin. The thickness of the outer nuclear layer (ONL) was measured at 10 locations at 2-mm intervals.

Immunohistochemistry

Freshly prepared rabbit eyes were fixed with 4% formaldehyde in phosphate buffer for 2 hours at 4°C. After fixation, the eyes were immersed in 20% sucrose, frozen in OCT compound (Sakura Finetechnical Co., Ltd., Tokyo, Japan), and sectioned at 15 μm. The tissue sections were processed for immunofluorescence staining with anti-rhodopsin antibody (RET-P1; Santa Cruz Biotechnology), followed by Alexa Fluor 488-conjugated anti-mouse IgG and Alexa Fluor 568-conjugated peanut agglutinin (PNA; Invitrogen), a lectin that binds specifically to rabbit cone photoreceptors.[29] Specimens were observed with a fluorescence microscope (BX61 microscope with digital photograph system DP70-BSW; Olympus, Tokyo, Japan).

Electron Microscopy

Eyes were enucleated from anesthetized rabbits (6-week-old WT and line 7 Tg rabbits). The anterior segment was removed, and the retina was fixed in 2.5% glutaraldehyde for 2 hours. After subsequent fixation in 1% osmium tetroxide for 90 minutes, the retina was dehydrated through a graded series of ethanols (50%–100%), and cleared in propylene oxide. Finally, the tissue was embedded in epoxy resin. Ultrathin sections were cut on an ultramicrotome (Ultracut E; Reichert-Jung, Vienna, Austria) and stained with uranyl acetate and lead citrate. The stained sections were observed by transmission electron microscopy (H-7650; Hitachi Co., Tokyo, Japan).

RESULTS

Generation of Tg Rabbits

We identified a rabbit rhodopsin BAC clone that included sequences approximately 150 kb upstream of the transcription initiation codon, the entire rhodopsin structural gene, and sequences downstream of the termination codon of the gene (Fig. 1A). Assuming that these genomic sequences would lead to correct expression of the rhodopsin gene, we inserted a C-to-T transition into the BAC clone in the codon of proline 347 by using BAC recombineering (Fig. 1B). The mutation introduced into the BAC Tg construct was then confirmed by sequence analysis (Fig. 1C). The C-to-T transition in exon 5 of the rabbit rhodopsin gene locus resulted in a proline-to-leucine substitution at codon 347.

After the BAC modification in *E. coli*, the linearized BAC Tg construct was purified and injected into rabbit embryos at the pronucleus stage. PFGE showed that the purified rhodopsin P347L Tg construct was approximately 150 kb (Fig. 2A). Southern blot analysis showed that 12 of 80 newborn rabbits (15%) were transgene positive, and 10 of the 12 survived (Table 1). These 10 founders were bred with WT rabbits, and six founders transmitted the transgene to their offspring.

Characteristics of Each Line of Tg Rabbit

FISH analysis showed that five founders, rabbits 7, 8, 10, 11, and 14, had a single site of transgene integration, and one founder, rabbit 16, had integrations at two sites (Table 2). Three lines, 10, 11, and 14, carried low copy numbers of the transgene, and two lines, rabbits 7 and 8, carried high copy numbers (Fig. 2B). The founder of line 16 carried both high and low copy numbers with transgene insertions on different

TABLE 1. Number of Animals and Zygotes Used to Generate Tg Rabbits

Donor rabbits (total)	36
Zygotes recovered (total)	800
Fertilized zygotes (%)	540 (68)
Zygotes microinjected (%)	456 (84)
Zygotes implanted (%)	456
Zygotes implanted per recipient rabbit (mean ± SD)	27 ± 3
Recipient rabbits	17
Pregnancy rate (%)	12 (71)
Gestation period (days, mean ± SD)	32 ± 1
Rabbits born (total)	80
Transgenic positive (F0) rabbit (surviving)	12 (10)
Founders that passed the transgene onto their offspring	6